Application of (U-Th-Sm)/He analysis in apatite: assessing the effect of salt structures on Sverdrup Basin rocks, Axel Heiberg Island, Nunavut

Robin Buckley

Submitted in Partial Fulfilment of the Requirements
for the Degree of Bachelor of Science, Honours
Department of Earth Sciences
Dalhousie University, Halifax, Nova Scotia
April 23, 2009

DALHOUSIE UNIVERSITY
Inspiring Minds

Department of Earth Sciences
Halifax, Nova Scotia
Canada B3H 4J1
(902) 494-2358
FAX (902) 494-6889

DATE: April 23, 2009

AUTHOR: Robin Buckley

TITLE: Application of (U-Th-Sm)/He analysis in apatite: assessing the effect of salt structures on Sverdrup Basin rocks, Axel Heiberg Island, Nunavut

Degree: BSc Honours Convocation: May Year: 2009

Permission is herewith granted to Dalhousie University to circulate and to have copied for non-commercial purposes, at its discretion, the above title upon the request of individuals or institutions.

Signature of Author

THE AUTHOR RESERVES OTHER PUBLICATION RIGHTS, AND NEITHER THE THESIS NOR EXTENSIVE EXTRACTS FROM IT MAY BE PRINTED OR OTHERWISE REPRODUCED WITHOUT THE AUTHOR'S WRITTEN PERMISSION.

THE AUTHOR ATTESTS THAT PERMISSION HAS BEEN OBTAINED FOR THE USE OF ANY COPYRIGHTED MATERIAL APPEARING IN THIS THESIS (OTHER THAN BRIEF EXCERPTS REQUIRING ONLY PROPER ACKNOWLEDGEMENT IN SCHOLARLY WRITING) AND THAT ALL SUCH USE IS CLEARLY ACKNOWLEDGED.

Abstract

In the Expedition Fiord region (c.a. 79°24'N / 90°50'W) of Axel Heiberg Island exposed evaporite diapir structures with associated perennial springs are present. These diapirs are rooted in a shallow allochthonous evaporite canopy that lies beneath this region. This study presents apatite (U-Th-Sm)/He thermochronologic data from the Expedition Fiord region for comparison with existing data from the eastern Sverdrup Basin. The apatite (U-Th-Sm)/He cooling ages of the regional data reflect exhumation cooling during the Eurekan Orogeny (ca. 45-65 Ma). In the vicinity of Expedition Fiord (U-Th-Sm)/He ages are considerably younger (ca. 32-41 Ma) indicating the rocks now at the surface cooled through He-retention temperatures (ca. 75 ± 15°C) ~10Ma later than rocks to the east in the Geodetic Hills region (ca. 48-61 Ma) as well as regional rocks. Data from this study are compatible with the thermal history previously suggested by apatite fission track-length modeling. Another result of this study is the identification of a significantly younger cooling age (13.9 ± 1.4 Ma) at the western edge of the study area in an island in Expedition Fiord.

A possible explanation for these data and anomalously young cooling ages is later exhumation of the rocks in the region of the canopy due to activity of the salt structure itself. It is also proposed that the effect may be due to the thermal effect of individual diapirs but the preferred hypothesis to explain the anomalously young data is a thermal effect that delayed cooling of the rocks in this specific area caused by the underlying salt canopy and heat advection by fluids.

Key Words: Expedition Fiord, apatite (U-Th-Sm)/He, salt canopy, perennial springs

Table of Contents

Table of Figures

Table of Tables

Acknowledgements

First of all I would like to thank my supervisor, Marcos Zentilli for the opportunity to work on such a stimulating project as well as his constant enthusiasm, guidance and patience that made this project possible. I would like to extend a special thank you to Jose Luis Antinao for teaching me some of the methods of this project. I would also like to thank Debra Wheeler and Keith Taylor from the Dalhousie Geochronology Centre for help with obtaining ages for the samples and explanations of their areas of expertise. Thank you also to Daniel Stockli from the University of Kansas for his U-Th-Sm work, Charlie Walls for his help with GIS, Pat Ryall for his comments and suggestions on earlier versions of this thesis and Eric Negulic for his suggestions and support as well as helping me understand the thermal effect of salt. Finally I must thank my parents for their patience and support as well as my classmates for their suggestions and humour.

CHAPTER 1: INTRODUCTION

1.1 General Statement

This thesis intended to test and confirm a paleogeothermal anomaly identified with preliminary geochronology data for rocks in the Sverdrup Basin near the head of Expedition Fiord of Axel Heiberg Island, northern Nunavut. Apatite fission-track ages were found to be younger in this area (meaning the rocks now at the surface cooled later) than the regional data for the Sverdrup Basin that indicate cooling during the Paleocene – Middle Eocene inversion due to the Eurekan Orogeny. Originally it was assumed that the young age effect was due to sample proximity to individual salt structures, which are known to funnel geothermal heat better than other rocks.

For this purpose the apatite (U-Th-Sm)/He method was applied on field samples collected from 2003 to 2008. The method dates the last time a rock cooled through a temperature of ca. 75°C. Results confirmed that the rocks in the study area cooled later than in the rest of the Sverdrup Basin, but the effect is more widespread than initially assumed, such that all rocks dated in the Expedition Fiord area yield relatively younger ages than the rest of the basin.

The study concludes that the most likely cause of the later cooling of the rocks is related to a salt canopy that underlies the head of Expedition Fiord, probably involving advection of fluids.

1.2 Questions to be answered

The questions that my thesis aimed to address were:

1) Can apatite (U-Th-Sm)/He thermochronology be used effectively to confirm relatively young ages (compared to the rest of the Sverdrup Basin) previously obtained with the apatite fission-track method near the head of Expedition Fiord, Axel Heiberg Island, Nunavut?

2) If confirmed, what is the cause of these young ages? Because salt conducts heat more efficiently than other sedimentary rocks, and this heat can have drastic effects on petroleum maturation, it would be very useful to have a method to measure and date the paleo-thermal effects of salt on rocks. Therefore, more specifically, could it be thermal effect from salt structures?

1.3 Study area location

Axel Heiberg Island, Nunavut is a northeastern island of the Canadian Archipelago and located within the Sverdrup Basin (Fig 1.1) centered near Latitude 79°24'N / Longitude 90°50'W. The basin consists of a thick section of Mesozoic sediments and on Axel Heiberg Island this package of sediments is 12-15 km thick (Jackson and Harrison, 2006). Approximately 180 oil wells were drilled in the Sverdrup Basin in the 1960s, and there is renewed interest in the hydrocarbons of this frontier basin, many of whose hydrocarbon resources are associated with salt diapirs (e.g. Arne et al. 1998). A Carboniferous-aged evaporite layer has, through halokinesis, formed an allochthonous salt canopy within the Sverdrup Basin. This salt canopy has associated salt diapirs, many of which are exposed on the surface. The well exposed salt structures make Axel Heiberg Island an ideal place to study the thermal effects of salt. It appears that the

salt structures at the surface level have affected the permafrost of the region and produced perennial springs with a temperature of 5°C (e.g. Zentilli et al. 2008).

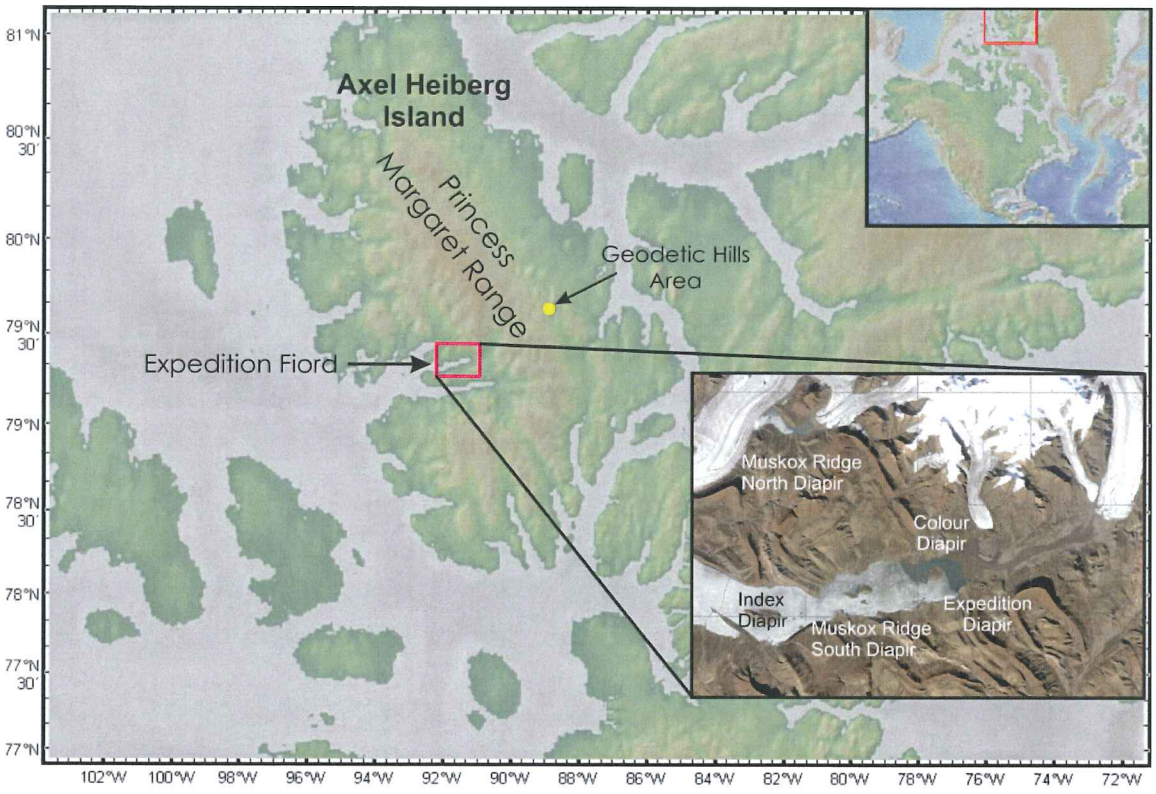

Figure 1.1: *Location Map: Axel Heiberg Island is located in the Canadian Arctic. The study area, Expedition Fiord, is located on western Axel Heiberg Island. Diapirs in the Expedition Fiord area have been labeled in the LandSAT image in the lower right corner.*

1.4 Previous work

During the late 1800's the first work in the Canadian Arctic Archipelago was completed as explorers began to push towards the North Pole (Trettin, 1989). Geological work in the Arctic became more prominent in the 1950's and the first stratigraphic outline of Canadian Arctic geology was published in 1955. A summary list of published literature relevant to this study can be found in Table 1.1. The remote location and ice cover of Axel Heiberg Island has impinged on Canada's ability to do research on this island and leaves many unanswered questions.

Year	Reference	Subject of Study
1961	Hoen, E.W.	Descriptions of salt diapirs in the Strand Fiord area.
1961	Kranck, E.H.	Descriptions of salt diapirs in the Strand Fiord area.
1963	Fricker, P.E.	Descriptions of salt diapirs in the Strand Fiord area.
1963	Kranck, E.H.	Descriptions of salt diapirs in the Strand Fiord area.
1966	Schwerdtner, W.M et al.	Structural development of evaporite diapirs on Axel Heiberg Island.
1966	Schwerdtner, W.M	Identification of evaporite diapirs formed under the influence of horizontal compression.
1967	Schwerdtner, W.M. and Clark, A.R.	Structural analysis of Mokka Fiord and South Fiord domes.
1969	Thorsteinsson, R. and Tozer, E.T.	Descriptions of the geology of the Arctic Archipelago.
1971	Thorsteinsson, R.	Geological Map compilation, Strand Fiord region, 1:250,000.
1975	Balkwill, H.R., Bustin, R.M., and Hopkins, W.S Jr.	Chronology of the Eurekan Orogeny.
1982	Balkwill, H.R., and Fox, F.G.	Overview of large-scale structures in the Western Sverdrup Basin.
1984	Schwerdtner, W.M. and van Kranendonk, M.	Structure of the Stolz Diapir - a well-exposed salt dome on Axel heiberg Island.
1984	van Berkel, J.T., Schwerdtner, W.M., and Torrance, J.G.	Descriptions of salt diapirs of the Sverdrup Basin.
1987	Ricketts, B.D.	Interpretations of the Princess Margaret Arch as well as the structural style of diapirs.
1988	Embry, A. and Osadetz, K.G.	Stratigraphy of volcanic rocks in the east-central Sverdrup Basin.
1988	Williamson, M-C.	Cretaceous igneous rocks of the Sverdrup Basin.
1989	Trettin, H.P.	Overview of the geology and tectonic history of the Arctic Islands.
1991	Davies, G.R. and Nassichuk, W.W.	Carboniferous and Permian history of the Sverdrup Basin.
1991	Embry, A.F.	Mesozoic history of the Arctic Islands.
1992	Stephenson, R.A., van Berkel, J.T., and Cloetingh, S.	Descriptions of salt diapirs of the Sverdrup Basin.
1998-2002	Arne, D. et al.	Apatite fission-track evidence for the timing of Eurekan deformation in the Sverdrup Basin
1999-2002	Pollard W. et al. & Andersen and Pollard	Descriptions and interpretation of perennial spring occurrences in the Expedition Fiord area.
2000	Chen, Z., Osadetz, K.G., Embry, A.F., Gao, H., and Hannigan, P.K.	Petroleum potential in the western Sverdrup Basin.
2003-2008	Zentilli, M.	Field work by M. Zentilli in Expedition Fiord Region.
2003	Villeneuve, M. and Williamson, M-C.	$^{40}Ar/^{39}Ar$ dating of mafic rocks from the Sverdrup Basin Magmatic Province.
2004	Williamson, M.C., Jackson, H.R., Villeneuve, M., Larsen, L.M., Zentilli, M.	Geochronology and Field Studies in the Canadian Arctic as applicable to hydrocarbon generation.

2005	Grist, A.M., and Zentilli, M.	Thermal history of the Nares Strait, Kane Basin, and Smith Sound region in Canada and Greenland.
2006	Jackson, M.P.A. & Harrison,J.C.	Study of the salt canopy on Axel Heiberg Island.
2006	Omelon,C. R., Pollard,W. H., Andersen, D. T.	Geochemical evaluation of perennial spring activity on Axel Heiberg Island.
2007	Jones, S.F., Wielens, H., Williamson, M-C. and Zentilli, M.	Impact of Magmatism on Petroleum Systems in the Sverdrup Basin.

Table 1.1 *Summary of previous work related to the geological mapping, stratigraphy and salt on Axel Heiberg Island.*

1.4.1 Previous (U-Th-Sm)/He work

A thermochronologic study of the low-temperature thermal history of the eastern Sverdrup Basin was completed by Grist and Zentilli (2005) who used the apatite fission-track and (U-Th-Sm)/He methods. The regional (U-Th-Sm)/He ages (Fig. 1.2) date the cooling of rocks through the 75°C isotherm and the youngest regional cooling age obtained (46.4 ± 3.7 Ma) coincides with the most recent tectonic event known to have affected Sverdrup Basin rocks, the Eurekan Orogeny (40-60 Ma).

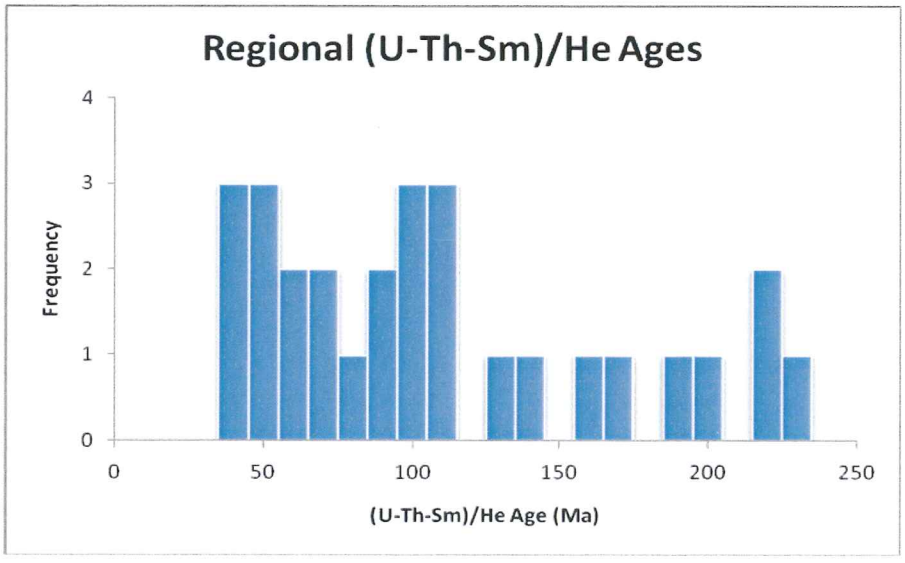

Figure 1.2: *Histogram of regional (U-Th-Sm)/He ages as determined by Grist and Zentilli (2005)*

1.5. Methods used

The method used for this thesis is the (U-Th-Sm)/He method and is discussed in Chapter 3. The steps followed for this method include; heavy mineral concentration, gem-quality crystal selection, He analysis using a mass spectrometer, U-Th-Sm analysis by the spiked ICP-MS method, calculation of ages and interpretation of ages.

1.6 Organization of Thesis

With the goals of determining whether the (U-Th-Sm)/He method can be used to detect the thermal effects of salt and the prevalence of this effect on central Axel Heiberg Island the thesis is organized as follows;

- Chapter 2 explains background on the thermal conductivity of salt, perennial springs on Axel Heiberg Island as well as the geology of the Sverdrup Basin.
- Chapter 3 explains the methodology of sampling, sample preparation and the (U-Th)/He method. It also summarizes the fission-track method as applicable to apatite and zircon.
- Chapter 4 gives the results of the (U-Th-Sm)/He dating and of the study.
- Chapter 5 discusses the work completed as well as the implications and interpretations.
- Chapter 6 provides the conclusion and gives recommendations for future work.

Chapter 2: Background Information

2.1 Geologic setting of the Sverdrup Basin

The Sverdrup Basin is a 1300 by 400 km elongate structural depression present in the Canadian Arctic (Fig. 2.1, Balkwill et al. 1983). The development of the Sverdrup basin was the main geologic process in the Canadian Arctic ongoing from the Late Carboniferous to Late Cretaceous (Davies and Nassichuk, 1991). The formation of the Sverdrup Basin began in the Late Carboniferous as a rifting event that lasted until the mid-Permian; this rifting was accompanied by basaltic volcanic activity (e.g. Jones et al. 2007; Jackson and Harrison, 2006). In the Sverdrup Basin, Paleozoic to Mesozoic strata overlie deformed Paleozoic strata (e.g. Jones et al. 2007; Figs. 2.2 and 2.3). The thickest section of these rocks is present in a 12-15 km thick section at the basin centre located on Axel Heiberg Island (Jackson and Harrison, 2006).

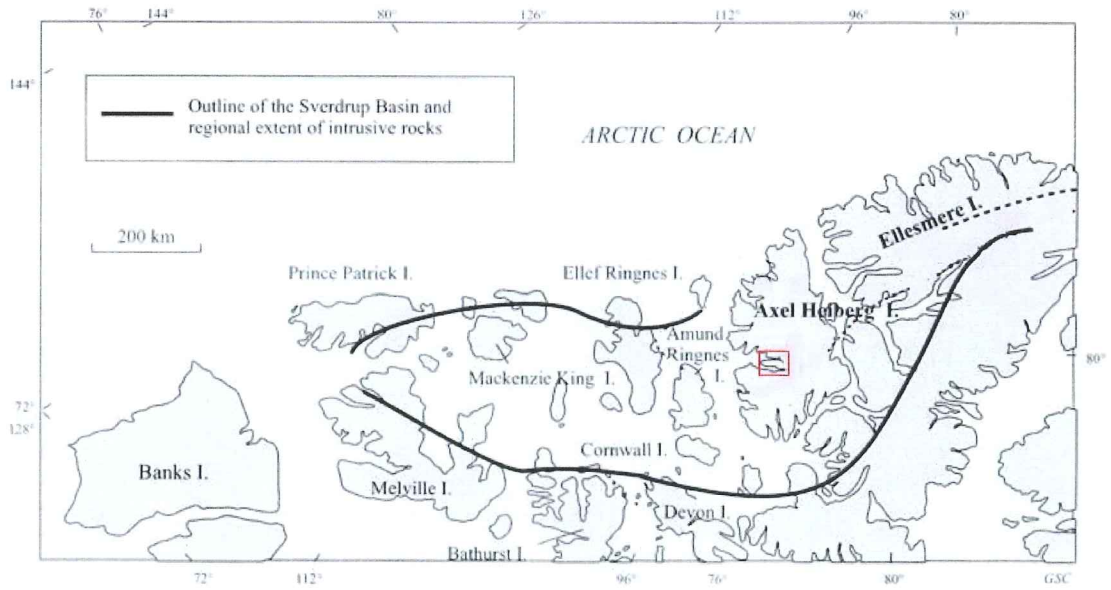

Figure 2.1: *Location of the Sverdrup Basin which is outlined in black within the Canadian Arctic Archipelago. Study area is shown in red box. Modified from Villeneuve and Williamson, 2003.*

The deposition of Sverdrup Basin sediments began during the very late Paleozoic as an estimated thirty transgressive-regressive cycles that reflect changes in subsidence,

eustatic sea level and sediment supply (Embry, 1991). The predominant deposition of clastic lithologies lasted until the Mesozoic Era although during the late Paleozoic Era evaporite and carbonate rocks were deposited as the basin began to develop (Trettin, 1989). One such unit, the Otto Fiord Formation, an upper Mississippian to Middle Pennsylvanian salt layer is particularly important as it was one of the earliest units deposited and facilitated the formation of salt structures during later stages of basin development (Embry, 1991; Davies and Nassichuk, 1991; discussed further in §2.3). Extrusive flood basalts of the Strand Fiord Formation were deposited during two major pulses of igneous activity (92-98 Ma and 127-129 Ma) during the Early Cretaceous; their feeder dykes and sills intruded Sverdrup Basin rocks at the same times (Villeneuve and Williamson, 2003). In the study area, the basaltic sills intruded pre-Triassic, Triassic, Jurassic and Cretaceous, as well as allochtonous evaporite bodies originating in the Carboniferous Otto Fiord Formation. The Eurekan Orogeny occurred during the Late Paleocene and Eocene (62-34 Ma) and was caused by the convergence of Greenland with Canada's Arctic (e.g. Arne et al. 1998). This "collision" caused shortening of the Sverdrup Basin and this effect is expressed by compressional structures, inversion and erosion of the sediments (e.g. Arne et al. 1998; Grist and Zentilli 2005; Jackson and Harrison, 2006). The Eurekan Orogeny is the most recent tectonic event to affect eastern Sverdrup Basin rocks and their thermal history. Yet, it is probable that salt structures are still rising in certain locations within Axel Heiberg Island, as hinted by Hoen (1961) and pointed out by Zentilli and Williamson (2004) and Jackson and Harrison (2006).

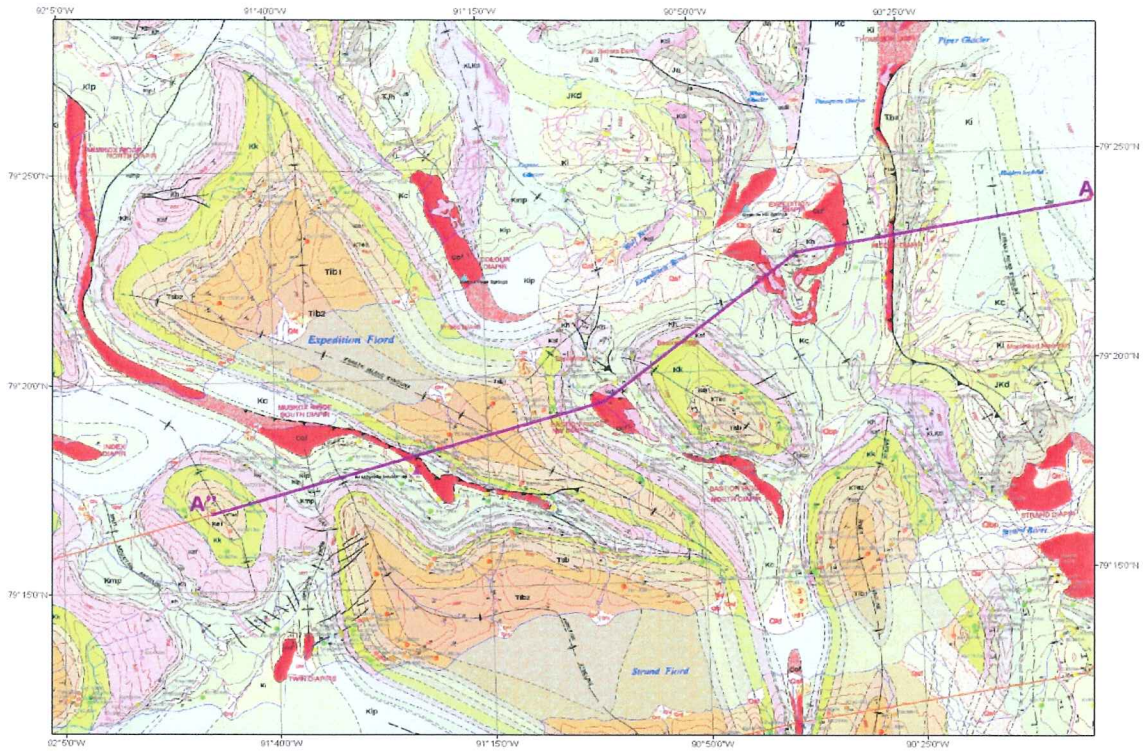

Figure 2.2: *Geologic Map of the study area, Expedition Fiord. For study area location see Fig. 1.1. For formation descriptions see Legend (Fig 2.4). For cross section A-A'' see Geologic Cross Section (Fig 2.3). Geologic map modified from Harrison and Jackson, 2008.*

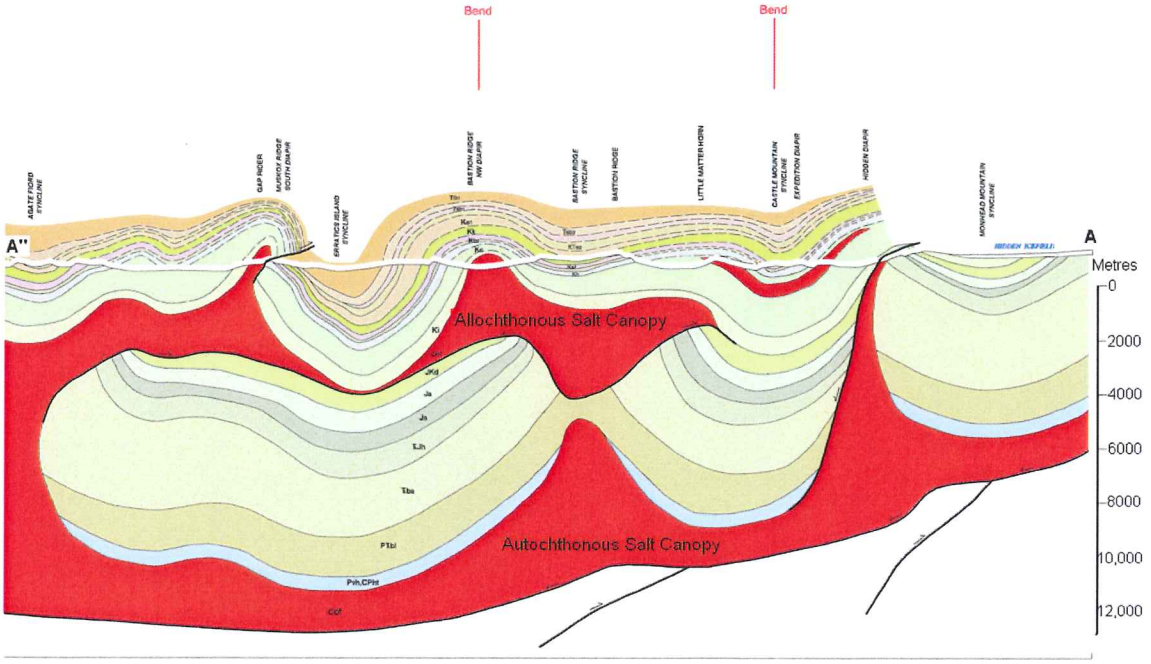

Figure 2.3: *Geologic Cross Section of the study area. Note the locations of salt canopies; salt structures are shown in red and the present day surface level is shown by the white line. For formations descriptions see text and Fig 2.4. Geologic cross section modified from Harrison and Jackson, 2008.*

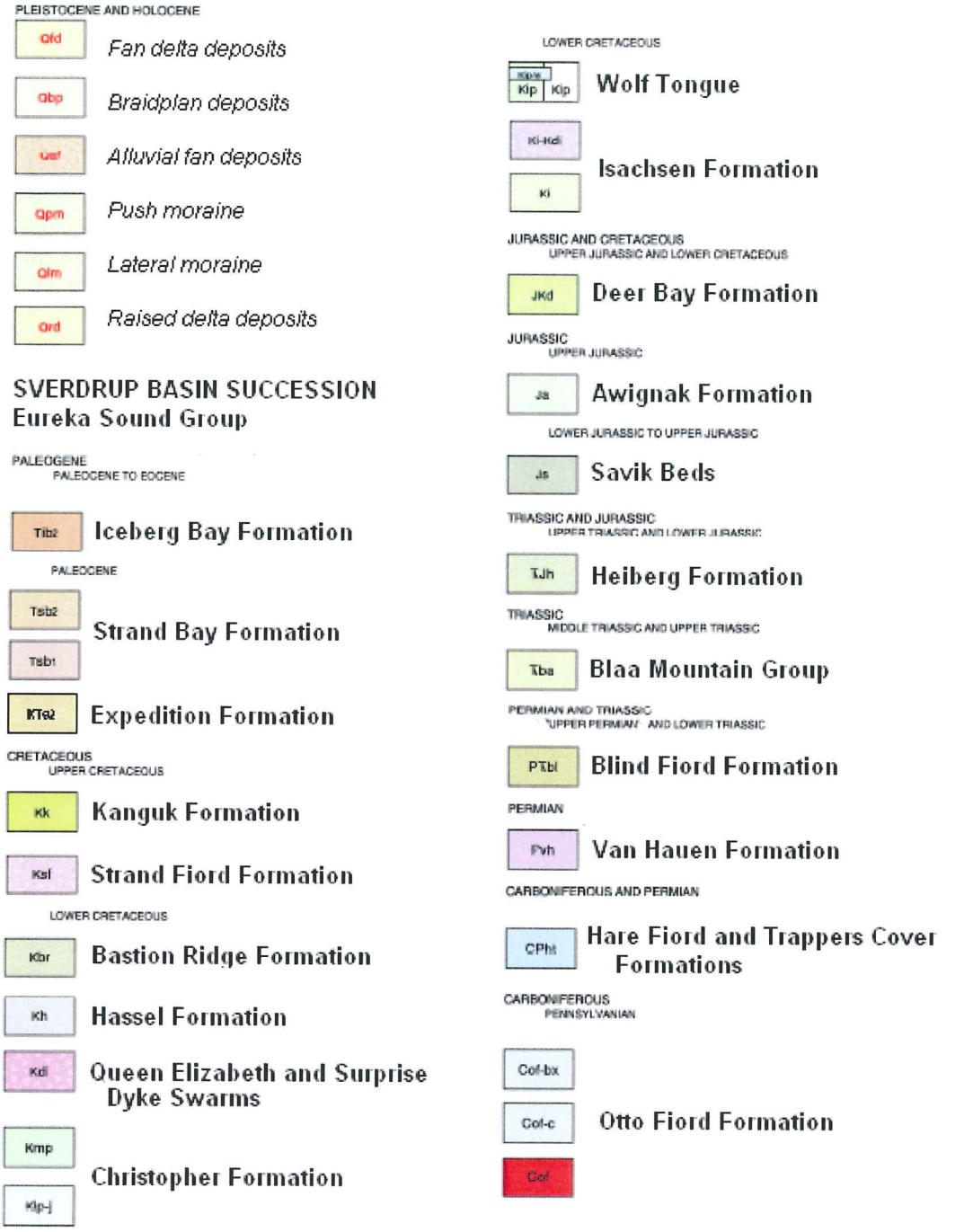

Figure 2.4: *Legend associated with geologic map and cross-section (Fig 2.2, 2.3) Modified legend from Harrison and Jackson, 2008. For lithological descriptions see section 2.2.*

2.2 Geologic Formations

The stratified rock formations (Figs. 2.2, 2.3 and 2.4) present in the Sverdrup Basin Succession on the surface of Expedition Fiord area from oldest to most recent include the Otto Fiord Formation, Blaa Mountain Group, Heiberg Formation, Savik Beds, Awingak Formation, Deer Bay Formation, Isachsen Formation, Christopher Formation, Hassel Formation, Bastion Ridge Formation, Strand Fiord Formation, Kanguk Formation, and the lower portion of the Eureka Sound Group (Harrison and Jackson, 2008). A brief description of each formation and an estimated thickness is provided with the exception of the Otto Fiord Formation which is described in section 2.4. The following stratigraphic description is modified from Lyon (2005) and written with reference to Fricker (1963), Thorsteinsson and Tozer (1969) and Harrison and Jackson (2008).

2.2.1 Blaa Mountain Group (Triassic)

This formation is composed of dark grey marine shales with minor siltstone occurrences. It is present in the Strand Fiord and Expedition area with a thickness of 700 m with a gradational contact with the overlying Heiberg Formation.

2.2.2 Heiberg Formation (Upper Triassic to Lower Jurassic)

The Heiberg formation is a sandstone with minor amounts of siltstone and shale that is mainly non-marine. In the region of the Strand Fiord, the Heiberg Formation is less than 1250 m thick and has an abrupt contact with overlying Savik beds.

2.2.3 Savik beds (Middle Jurassic)

These beds of marine origin contain shale with minor amounts of siltstone and clay ironstone. On Axel Heiberg Island, the thickness ranges from 80 to 300 m and there is a gradational contact with the Awinkgak Formation.

2.2.4 Awingak Formation (Upper Jurassic)

The Awinkgak formation consists of mainly non-marine quartz arenite sandstones and shales with varying thicknesses of 75 to 300 m and has a gradational contact with the Deer Bay Formation.

2.2.5 Deer Bay Formation (Upper Jurassic to Lower Cretaceous)

This marine formation consists of shale, siltstone, and minor sandstone, has a thickness of 80-700 m, and has a gradational contact with the Isachsen Formation.

2.2.6 Isachsen Formation (Lower Cretaceous)

The Isachsen formation is composed of sandstone with a range of grain sizes and the upper part consists of shale that is commonly intruded by dykes and sills. The contact with the overlying Christopher Formation is gradational.

2.2.7 Christopher Formation (Lower Cretaceous)

Grey shales dominate this formation with minor amounts of sandstone and siltstone. The thickness of this unit is as much as 1000 m with intruding sills and dykes. The Christopher Formation is superimposed on the Hassel Formation forming a gradational contact.

2.2.8 Hassel Formation (Lower Cretaceous)

The Hassel Formation is marginal marine-nonmarine and includes medium to fine grained quartzose sandstone and siltstone. Along Axel Heiberg Island, the thickness can reach 430 m and has a gradational contact with the overlying Kanguk Formation.

2.2.9 Bastion Ridge Formation (Lower Cretaceous)

This marine formation consists of shale and silty shale with minor siltstone and sandstone. This unit ranges from 5 to 242 m thick on Axel Heiberg Island. This formation is non-conformably overlain by the Strand Fiord Formation.

2.2.10 Strand Fiord Formation (Upper Cretaceous)

This formation consists primarily of basalt deposited in subaqueous and subaerial environments with minor diabase sills and mafic pyroclastic rocks. On Axel Heiberg Island the unit has a maximum thickness of 701 m. This formation is non-conformably overlain by the Kanguk Formation.

2.2.11 Kanguk Formation (Upper Cretaceous)

The Kanguk Formation consists of shales, with minor siltstone, sandstone and a couple bentonitic tuff beds. The Kanguk Formation has a maximum thickness of 243 metres and has a gradational contact with the overlying Eureka Sound Group.

2.2.12 Eureka Sound Group (Upper Cretaceous to Cenozoic)

This group consists of the Expedition Formation, Strand Bay Formation and Iceberg Formation. These formations consist of coarse and fine continental clastics and contain lignite and coal layers. They are locally several hundred meters thick, and the maximum thickness along the Strand Fiord area is 2900 m.

2.2.13 Buchanan Lake Formation (Early Tertiary)

This formation does not appear in the map above, but occurs to the Northeast of the Stolz Thrust in the Geodetic Hills area. It has a Middle Eocene age and it consists of conglomerates, sandstones and coal (Harrison et al. 1999).

2.3 Salt

The thermal conductivity of salt is known to be 2-3 times greater than that of other sedimentary rocks (Table 2.1; e.g. Yu et al. 1992). The contrast in thermal conductivity between salt and its surroundings will result in higher geothermal gradients and heat flow above the salt when compared with adjacent sediments (e.g. Keen, 1983; Fig 2.5). In addition, beneath salt structures, negative temperature anomalies are expected (Yu et al. 1992).

Lithology	Thermal Conductivity Wm/°C
Halite	5.5
Anhydrite	5.5
Limestone	2.8-3.5
Sandstone	2.6-4.0
Shale	1.5-2.9
Coal	0.3
Granite	2.5-4.5
Andesite	3.0-4.0
Basalt	4.0-5.0
Peridotite	4.0-6.0

Table 2.1: *Thermal conductivities of various lithologies present in the Sverdrup Basin. Note the significantly higher thermal conductivity of evaporite deposits, halite and anhydrite, in comparison to other sedimentary rocks. Thermal conductivity values from Evans, 1977.*

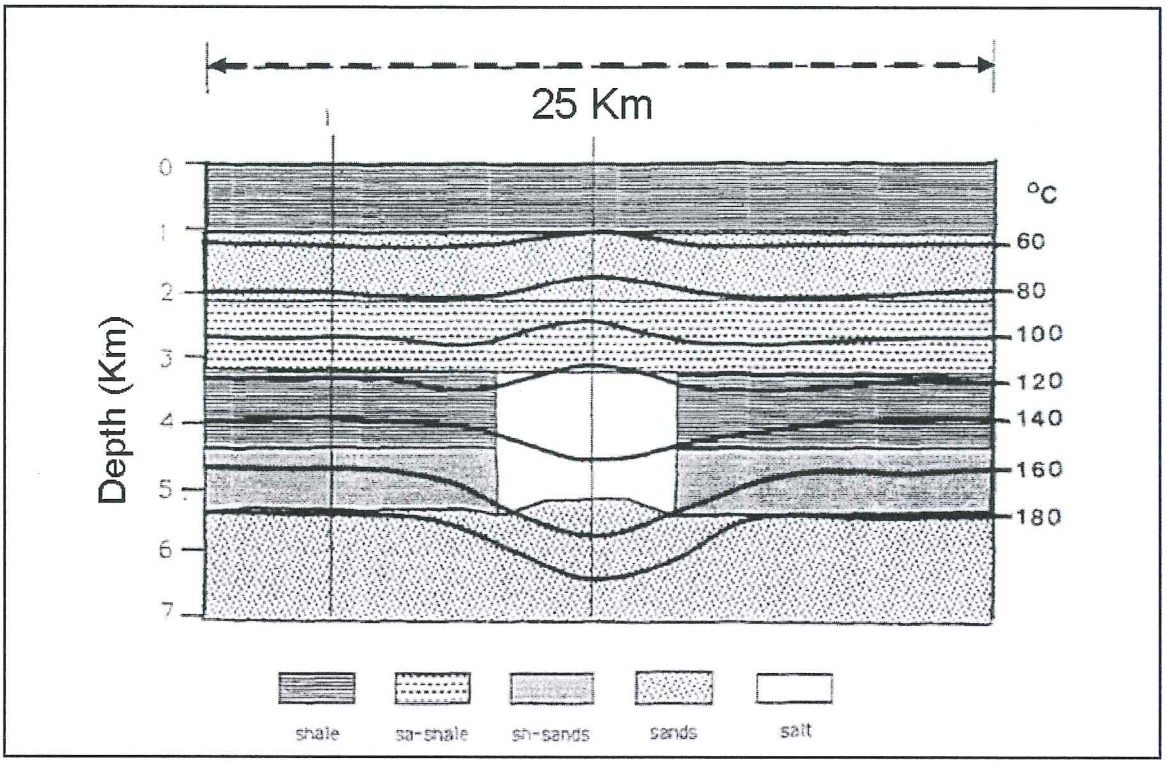

Figure 2.5: *Temperature distribution around salt body showing increased temperature above salt body and decreased temperature beneath (figure from Yu et al. 1992).*

High geothermal gradients are commonly considered advantageous for the thermal maturity of petroleum source rock (Keen, 1983). Therefore, studies of petroleum generation in sedimentary basins have suggested that because thermal maturity is important for petroleum generation, salt diapirs can provide an important contribution to this maturity within the sediments that rest above them.

2.4 Evaporite Deposits

The Otto Fiord Formation was initially deposited on Axel Heiberg Island as a thick layer of salt that accumulated during Carboniferous rifting on top of stretched Paleozoic and Proterozoic crust at a paleolatitude of 27-32° (Jackson and Harrison, 2006). Since its initial deposition the Otto Fiord Formation has undergone significant

deformation, due to tectonic as well as depositional events, most notably in the area of present day western Axel Heiberg Island. This is reflected by the exposed salt diapirs present today.

Diapirs initially began rising no later than the early Triassic (250 Ma) and Jackson and Harrison (2006) suggested that two likely mechanisms to explain this diapir rise are (1) reactive diapirism as a response to rift-related extension or (2) differential loading by prograding sediments of a Carboniferous carbonate shelf. Stratigraphic thinning and onlap against diapirs stratigraphically record the breakout of diapirs as do diapir flanking unconformities. A sediment supply hiatus during the early Cretaceous period allowed the exposed salt diapirs of the Otto Fiord Formation to be eroded and spread into a sheet that coalesced to form an allochthonous salt canopy (Fig. 2.4). This canopy was later onlapped and covered by the Lower Cretaceous fluvial-deltaic Isachsen Formation and subsequent Cretaceous-Paleogene rocks which also filled in any depressions that existed in the canopy. This allochthonous shallow salt canopy acted as a detachment layer for Paleogene Eurekan Orogeny folds and as source layer for a second generation of diapirs which were formed, exhumed and exposed during the Eurekan Orogeny.

The diapirs composed of this salt consist of nodular anhydrite that have been or are currently weathering to a gypsum skin (Jackson and Harrison, 2006). The diapirs have minor carbonate interbeds which are commonly brecciated. At depth the diapirs are commonly composed of halite. For this reason, the term salt is used as a general term in this thesis.

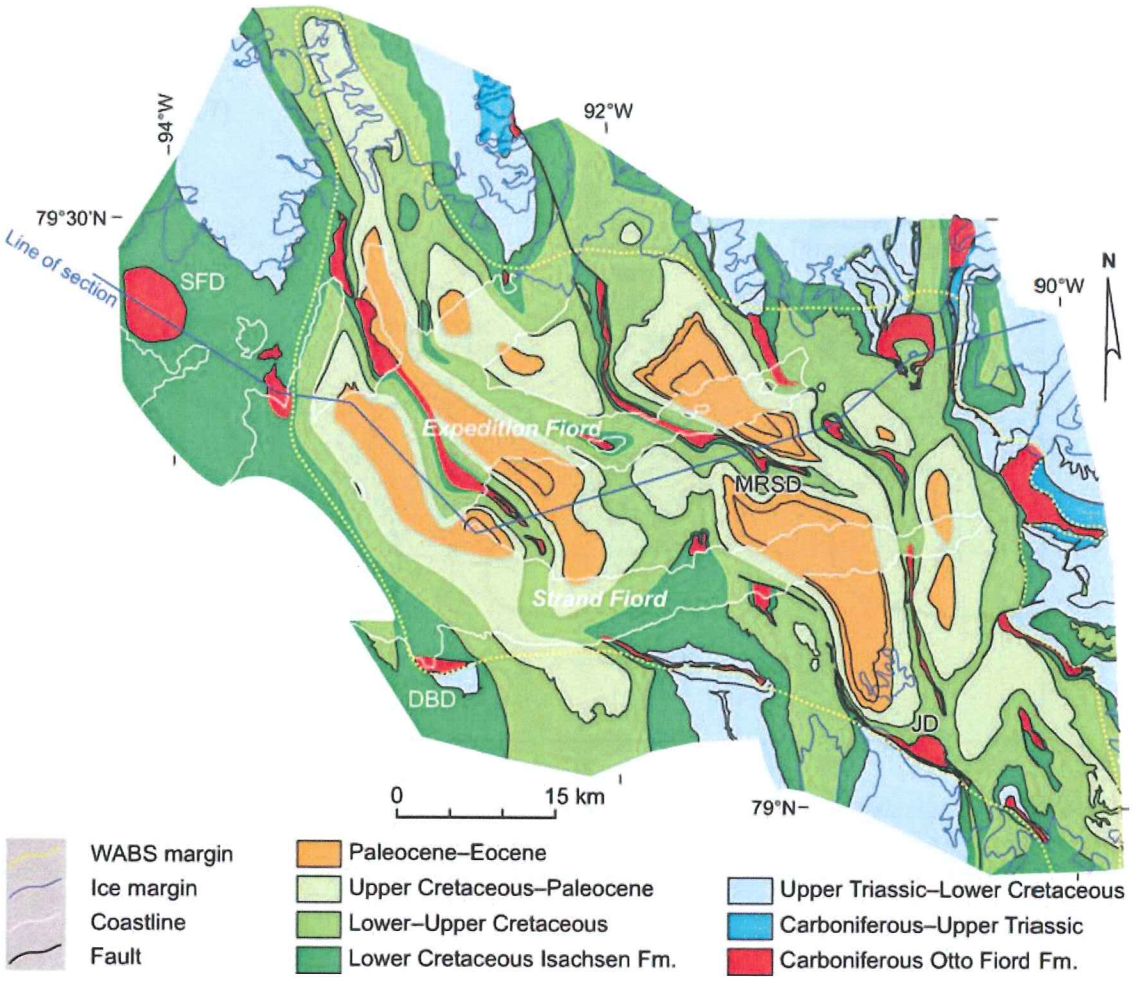

Figure 2.6: *The boundary of the allochthonous salt canopy present in the Expedition Fiord area is shown by yellow line as described by Jackson and Harrison, 2006. Figure from Jackson and Harrison, 2006.*

2.5 Perennial Springs Associated with Diapirs

On western Axel Heiberg Island at Expedition Fiord perennial springs occur adjacent to two exposed diapirs; Colour Peak and Gypsum Hill (Pollard et al. 1999; Figs. 1.1 and 2.3). The springs flow at a constant rate year-round and these springs occur in a region with an annual mean temperature of -15°C and 600m of permafrost (Andersen et al. 2002).

A model proposed by Andersen et al. (2002) describes the perennial springs as a glacial phenomena with the springs sourced by glacial lakes that flow through the salt structures (Fig. 2.7).

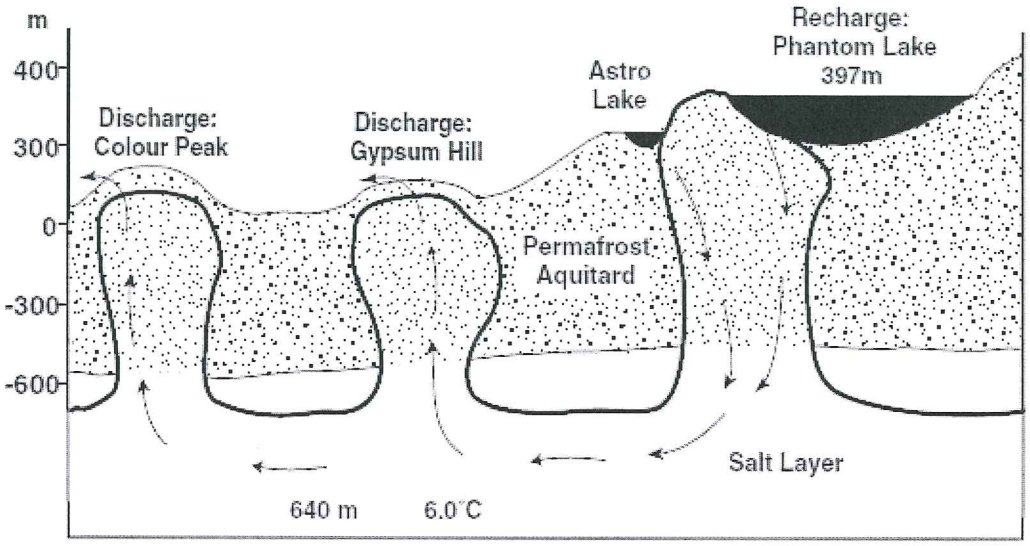

Figure 2.7: *Model by Andersen et al. describing source for perennial springs as a glacial lake. The arrows show the direction of water flow through a diapir down below the permafrost layer where the temperature is calculated to be 6°C due to the sub-permafrost geothermal gradient. Figure from Andersen et al.*

The above model (Fig 2.7) is based on a Quaternary geology approach, led by the Geography Department at McGill University. However, the Dalhousie project followed a basinal thermal point of view when designing the Axel Heiberg Island project, based on thermal effects of salt in the Atlantic margin of Nova Scotia. In this context it is relevant to point out a study by C. Keen (1983), who suggested that fluids might be involved in the proximity of salt diapirs, to explain sharp heat flow anomalies encountered in the Primrose structure offshore Atlantic Canada.

Keen studied the anomalous heat flux found over the Primrose structure and concluded that advective hot fluid motions over top of the diapir could provide sufficient

heat for a long enough time to produce the observed thermal maturity in the sediments at this site while she reckoned that conductive heat was not sufficient to explain the thermal anomalies. Keen's model was based on the fact that during active diapirism a zone of mechanical incompetence and fracturing should be created in the sediments adjacent to the salt structure which could provide a pathway for hot fluids to quickly migrate to the top of the diapir from deeper hotter levels.

CHAPTER 3: MATERIALS AND METHODS

3.1 Sampling Strategy

The samples used for this study were collected by Marcos Zentilli of Dalhousie University during field seasons in 2003, 2005, 2007 and 2008. The purpose was to obtain a representative suite across the 2000 m high Princess Margaret Mountain Range, from sea level along Expedition Fiord through Eureka Pass, across a major thrust fault system (the Stolz Thrust) and into the foreland basin of that fault system in the Geodetic Hills area (Fig. 1.1). One objective was to date the movement of the Stolz Thrust, following a similar study further east in the Sverdup Basin (Arne et al. 1998; Arne et al. 2002, Grist and Zentilli 2005; 2006). Another objective was to detect any thermal effects caused by evaporite (salt, anhydrite) structures.

Where possible, samples were obtained from diabase (basalt) sills and dykes which are described in section 3.2 and are known to have intruded the strata during two short events: ca. 92 and 129 Ma (Villeneuve and Williamson, 2003). This selection would ensure that apatite collected would be of consistent chemistry and texture (euhedral crystals), and its age (Cretaceous) known. Where intrusions were not present, sandstones were sampled; but the apatite in sandstones may have different ages and provenances. These grains have different chemistries which may affect helium gas diffusion, and are rounded or broken during erosion-sedimentation cycles; these features make important volume and shape corrections difficult (see section 3.8). Sandstone samples near sills were expected to have been thermally reset by the hot intrusions (e.g. Jones et al. 2007). Samples from rocks in close proximity to extruded salt diapirs exposed on Axel Heiberg Island were obtained specifically to determine if these rocks were thermally affected.

Each sample was labeled and brought back to the Dalhousie Geochronology Centre for processing.

In thermochronological studies it is not uncommon that a large proportion of the samples collected in the field are "unsuccessful", meaning they do not yield datable minerals in sufficient quality and quantity. A sample with abundant crystals that are euhedral and of sufficient size is ideal in order to select crystals with the ideal geometry and without inclusions. It was expected that about half of the samples would have a sufficient quantity of gem quality apatite crystals to obtain an age for the samples using apatite (U-Th-Sm)/He analysis. The locations of samples that were obtained are shown in Figure 3.1.

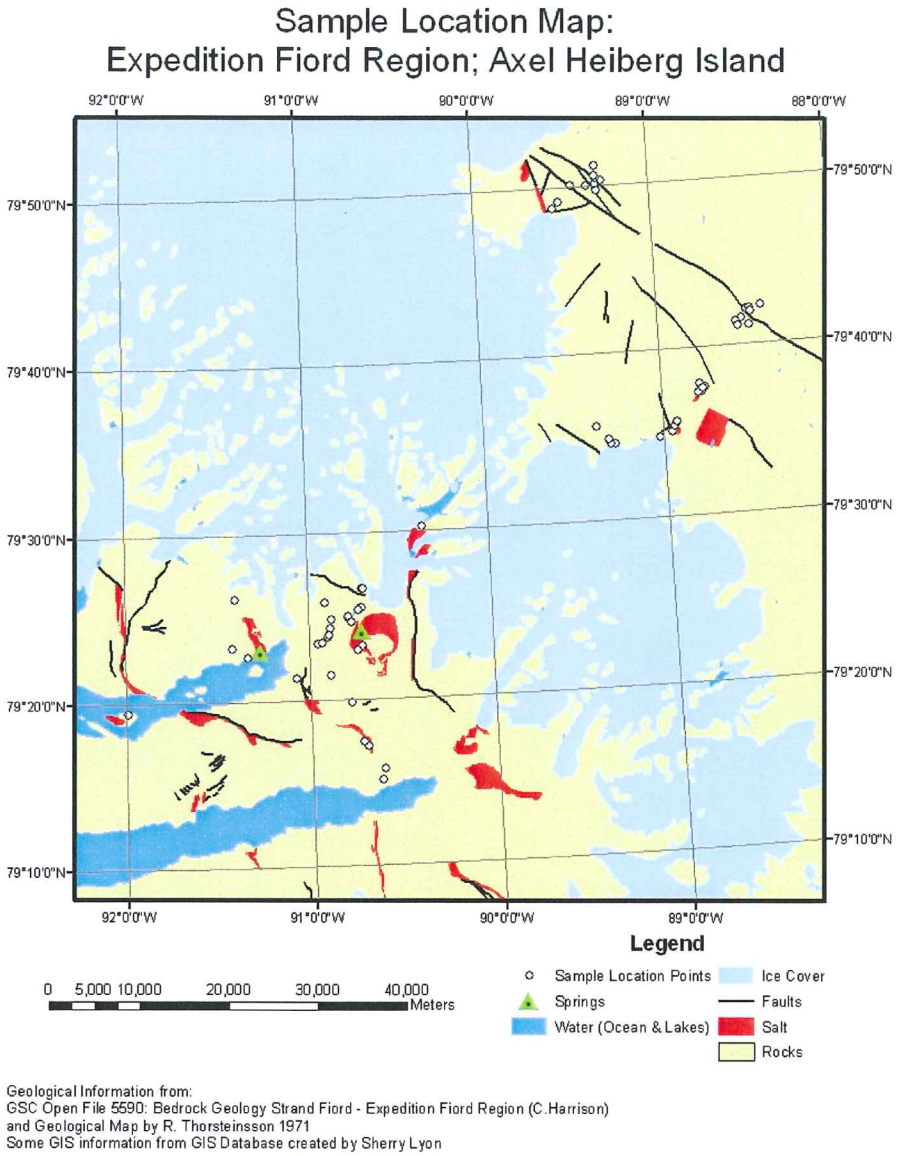

***Figure 3.1**: All samples obtained by Marcos Zentilli for thermochronologic studies of Axel Heiberg Island.*

3.2 Sample Description

The tholeiitic basalts that were sampled in the Expedition Fiord and Geodetic Hills areas of the Princess Margaret Range were described by Jones (2006) and Lyon (2005). They found that the very fine to medium grained dykes and sills from this area showed similar mineralogy and textures. The dominant mineralogy present in all samples consists of plagioclase, clinopyroxene and Fe-Ti oxides with grain size ranging from very

fine to medium. Texturally, the samples are generally inequigranular, aphyric and show varying degrees of alteration. Olivine grains are often present and have alteration rims or alteration to iddingsite within the grain itself. Biotite, chlorite, amphibole, iddingsite, saussurite, sericite, carbonate and clays are all secondary minerals found in the dykes and sills. Euhedral apatite is present in the samples as an accessory mineral within both the sills and dykes and zircon is found within biotite grains.

3.2 (U-Th-Sm)/He Thermochronology

The (U-Th-Sm)/He method was a technique developed during the early 1900's for dating geologic material, but was considered unreliable due to the profuse diffusion of radiogenic He out of imperfect host minerals (e.g. Grist and Zentilli, 2004).

The decay of radioactive elements can be used as a dating method if assumptions about the initial proportion of daughter products are made. U-238 decay series is commonly used for this purpose as after time it and some of its radioactive daughter products emit stable alpha particles (He).. Measuring the isotopic proportions of parent and daughter isotopes can give estimates of the age at which crystals closed to diffusion of these daughter isotopes out of the crystal structure (Ehlers and Farley, 2003). Although it is rarer than alpha emission, uranium also decays by spontaneous fission and the remains of this spontaneous fission are recorded as a fission-track. Fission-track measurements can also be used as a method to obtain crystal ages and this is discussed further in section 3.3.

There are a variety of techniques and applications for (U-Th-Sm)/He thermochronology which involve establishing the cooling histories of rocks (Farley, 2002). To estimate He production over time (t), the following equation is used:

$$^{4}He = 8\ ^{238}U\ (e^{\wedge}(\lambda_{238}t) - 1) + 7\ (^{238}U/137.88)\ (e^{\wedge}(\lambda_{235}t) - 1)$$
$$+ 6\ ^{232}Th\ (e^{\wedge}(\lambda_{232}t) - 1) + {}^{147}Sm\ (e^{\wedge}(\lambda_{147}t) - 1)) \quad (3.1);$$

where λ is the decay constant for the parent atoms ($\lambda_{238} = 1.551 \times 10^{-10}\ y^{-1}$, $\lambda_{235} = 9.849 \times 10^{-10}\ y^{-1}$, $\lambda_{232} = 4.948 \times 10^{-11}\ y^{-1}$, $\lambda_{147} = 6.539 \times 10^{-12} y^{-1}$) and **t** is the time (years) He has been accumulating in the mineral (Farley, 2002).

Apatite crystals make a good low temperature thermochronometer because their structure closes to He diffusion at ~75°C (Farley, 2002; Ehlers and Farley, 2003). The temperature range between ~80-40°C is considered the partial retention zone (PRZ) because as an apatite crystal cools through this temperature zone He atoms begin to accumulate within the crystal and partial diffusion of He takes place (Fig. 3.2). The apparent closure temperature of an apatite crystal depends on the amount of time spent within the PRZ and the radius of the apatite crystal (Farley and Stockli, 2002).

The lower closure temperature of apatite to He diffusion makes it possible to detect cooling on a smaller scale that may be tectonically induced in comparison to high temperature systems that cannot record these small variations (Ehlers and Farley, 2003). In the upper few kilometers crustal isotherms will mimic surface topography, more notably so in close proximity to the surface which means that the lower the closure temperature of a system the greater the effect of topography (Fig. 3.2). Also apatite He ages are strongly influenced by perturbations in the shallow crust's thermal field and will be affected if relief is changing during their exhumation or if the exhumation rate is changing (Braun, 2002).

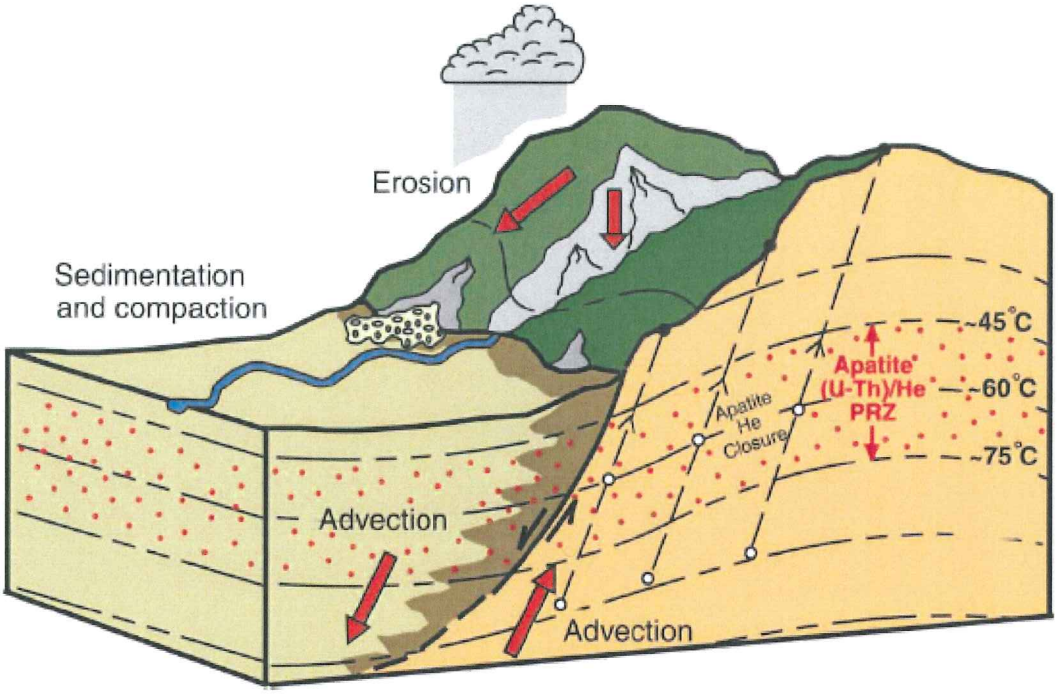

Figure 3.2: *Thermal processes that will influence (U-Th-Sm)/He ages. The isotherms will mimic surface topography as shown. Apatite will retain some but not all helium during the time spent within the partial retention zone (PRZ). Figure from Ehlers and Farley, 2003.*

Rocks normally remain at temperatures greater than 75°C to depths of about 2-4 km depending on the geothermal gradient, therefore, apatite's (U-Th-Sm)/He closing temperature of ~75°C makes it a preferred thermochronometer for shallow crustal studies of thermal character such as burial, uplift, exhumation and erosion (Ehlers and Farley, 2003). The rocks present on Axel Heiberg Island should have cooled through this temperature as they were exhumed by the Eurekan Orogeny. As salt structures are known to cause thermal anomalies and high geothermal gradients, rocks overlying salt structures may have delayed cooling through the 75°C isotherm and later closure to He diffusion than rocks that do not overlie salt structures (Fig. 3.3.) This should cause apatite crystals in rocks that overlie salt structures to have younger He ages than crystals from rocks not underlain by salt structures.

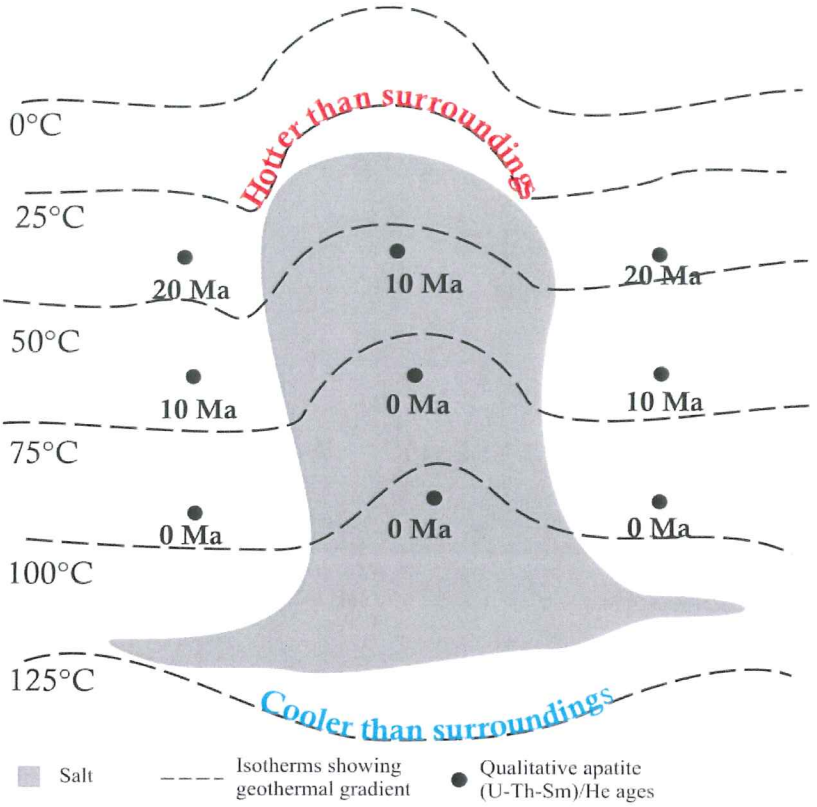

Figure 3.3: *Schematic diagram of a salt diapir showing how geothermal gradients change with proximity to a diapir as well as how apatite (U-Th-Sm)/He dates vary with proximity to a diapir.*

3.3 Apatite Fission-Track Thermochronology

The apatite fission-track method has been widely used to constrain low-temperature thermal histories (Donelick et al. 2005). The natural, spontaneous fission of unstable elements will cause linear damage to the lattice structure of the host mineral, these are called fission-tracks and the analysis of fission-tracks can be used as a thermochronological technique (Juez-Larré, 2003). The "ion spike model" describes the formation of fission-tracks as the fission decay causes a nucleus to split in two parts, a heavier and a lighter piece, that are positively charged and this process releases a large amount of energy. This energy primarily takes the form of kinetic energy as the two fragments repel and travel away from each other their energy is consumed as a result of

nuclear collision and electrical interaction. The resulting structural damage and ionization is called a fission-track.

Fission-tracks are only preserved in insulating materials with no free moving electrons that would cause the damaged charged zone known as the fission-track to quickly repair itself (Juez-Larré, 2003). Over time fission-tracks will be naturally healed by the host mineral; this process is called annealing and is affected by temperature. Below a certain temperature (closure temperature) the fission-track is effectively maintained, whereas, above this temperature the tracks are irreversibly and incrementally erased due to annealing (Juez-Larré, 2003). By knowing the number of fission-tracks, their lengths and the amount of U-238 present in a crystal, knowledge about the crystal's cooling age can be obtained (Juez-Larré, 2003).

For apatite crystals reduction of track length by annealing of fission damage occurs significantly at temperatures of about 50-60°C over very slow cooling rates and is essentially complete at about 100-150°C (e.g. Grist and Zentilli, 2005). Therefore apatite fission-track ages date the cooling of a rock through 100°C. The closure temperature for the geological annealing of zircon fission-tracks is estimated to be 240 ± 50°C for a cooling rate of 10°C/Ma and 194 ± 18°C for a cooling rate of 0.46°C/Ma (Juez-Larré, 2003). Within the project, apatite fission-track dating was carried out in the Dalhousie Fission-track Research laboratory between 2003 and 2007 by A. Grist. Fission-track dating in zircon of samples from the same area referred to in this chapter were done by P. O'Sullivan of Apatite to Zircon, Inc., of Moscow, Idaho, USA (Zentilli in prep.). Apatite fission-track cooling ages can be used in combination with apatite He ages to more tightly constrain cooling histories and support interpretations (Farley, 2002).

3.4 Physical Processing of Samples

In order to isolate the apatite crystals to be used for (U-Th-Sm)/He analysis from the rest of the whole rock samples physical processing was completed by members of the Dalhousie Geochronology Centre. A detailed description of the basic mineral separation techniques used in the Dalhousie Geochronology Centre is given by Grist and Zentilli (2004).

The first step involved crushing, grinding and then sieving 800 g aliquots of the whole rock samples in order to isolate grains of sufficient size (>30 μm). In cases where large volumes of rock were isolated at the end of this process a Wilfley water table was used to further separate the sample on the basis of specific gravity, the heavier part of the sample was used in the next stage of processing. The next stage of processing was separation based on specific gravity (SG) using heavy liquids, sodium polytungstate, which has a specific gravity of 2.8 g/cm^3 is used in the Dalhousie Geochronology Centre. When grains of rock are placed in this liquid apatite crystals (SG 3.15-3.20 g/cm^3) should sink, whereas, quartz (SG 2.65 g/cm^3) and other less dense minerals should float. The isolated fraction of sample was then separated on the basis of magnetic properties using a Frantz Isomagnetic separator. After these processes the remaining sample consists primarily of apatite and zircon.

3.5 Apatite Crystal Selection and Preparation

The most important but most time consuming part of the (U-Th-Sm)/He analysis process is the selection of high quality apatite crystals from each sample in order to achieve an adequately precise age. The best crystals were selected for further analysis on

the basis of size, symmetry, number and size of imperfections and overall clarity of the crystal.

To isolate the highest quality apatite crystals from the remaining portions of rock after the physical processing of the samples, the first step is to observe and isolate the grains under a Stemi SV11 Zeiss binocular microscope. This is done at low powers of magnification (35.2-105.6X) and the most important aspects for crystal isolation at this stage are the overall crystal shape and size. Crystal size and symmetry are relevant during the selection process as they will affect the accuracy and amount of error incorporated by the F_T correction and alpha particle ejection models (§ 3.8; Ehlers and Farley, 2003). Crystals were considered to have adequate symmetry if the length to width ratio was 2:1 or greater with the largest possible radius. The minimum suggested radius is 60 μm in order to minimize the F_T correction.

In order to correct measured He ages with the F_T correction measurements of the crystal length and of the width of the three short axes of the hexagonal shape were obtained (Fig. 3.4). Grains were photographed and measured using a PaxCAM and PaxIt software which enable real time calibrated measurement of crystal axes lengths.

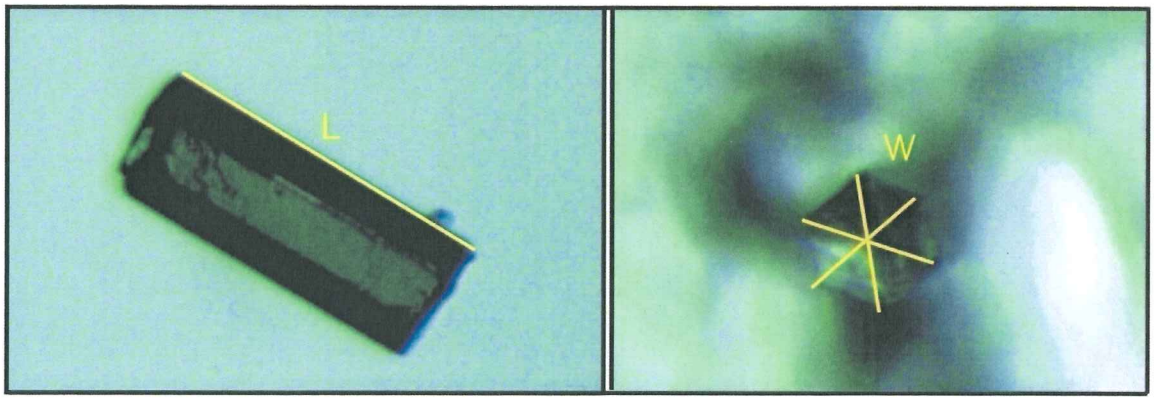

Figure 3.4: *Example of an apatite crystal (FT05-034b-4) and the measurements that were obtained during the selection process (indicated in yellow). These dimensions are also used in calculating the crystal's surface area to volume ratio for the F_T correction. (See § 3.8)*

Crystals that met the size and symmetry standards were rejected if they contained imperfections. Imperfections included small bubbles within the apatite crystals that may be an unwanted source of parent and daughter atoms (Fig. 3.5). The bubbles may contain He isotopes from another source with an unknown proportion and amount of He atoms would give an inaccurate age determination. Mineral inclusions that may be found in apatite such as monazite, and zircon are rich in U-Th-Sm, and can yield an incorrectly old (U-Th-Sm)/He age by producing "parentless" He. As many inclusion phases survive the HNO_3 dissolution so the amount parent nuclei from the inclusion will not be measured (Farley, 2002; Vermeesch et al. 2007). In order to examine crystals for these imperfections they were observed and photographed under higher magnifications with a Zeiss Axioplan binocular microscope at 44-400X magnification. The samples that met the symmetry and size standards and were deemed to be void of significant inclusions were ready to be loaded into platinum crucibles for heating and gas extraction.

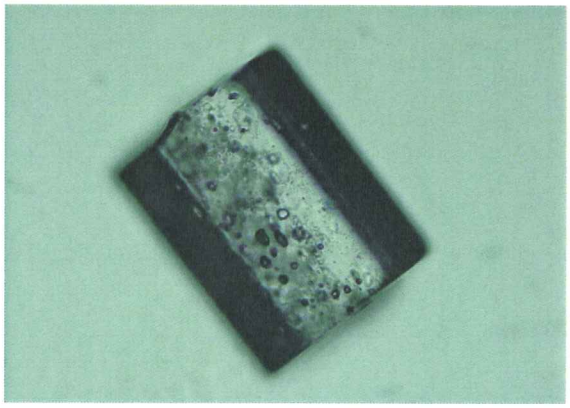

Figure 3.5: *An example of an apatite crystal that was rejected during the selection process due to abundant inclusions.*

Platinum micro-crucibles are hollow, open-ended cylinders of platinum with a length of 1mm and diameter of 0.5mm (Fig. 3.6). Platinum cylinders are used for this procedure as platinum has a high melting point (1768°C), low hydrogen content, and

malleability but the platinum can cause interferences with the Th^{232} measurement when the platinum crucible is dissolved during the U-Th-Sm analysis (further discussed in § 3.7, Evans et al. 2005). Once each crystal has been enclosed in a platinum crucible the samples are ready for a measurement of the proportion of He gas by heating and mass spectrometry.

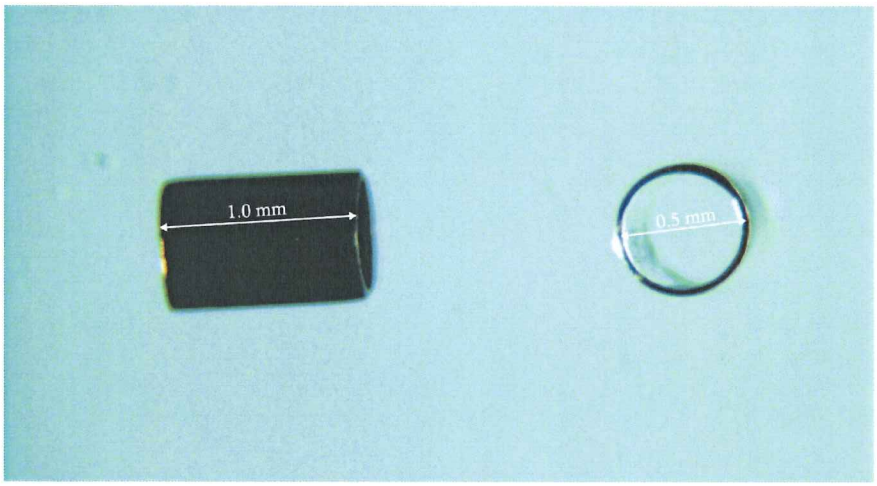

Figure 3.6: *Platinum micro-crucible used for holding apatite crystals during He gas extraction. Dimensions are shown in white.*

3.6 Helium Gas Extraction: Mass Spectrometry

In order to obtain an accurate (U-Th-Sm)/He age the amount of ^4He present in each apatite crystal must be measured precisely. The measurements for this study of ^4He were completed by the He mass spectrometer in the Dalhousie Geochronology Centre - Noble Gas Lab which is operated by Keith Taylor. The process includes heating the sample with a laser, vacuo extraction, purification, spiking with a known spike of ^3He, analysis of the $^3He/^4He$ ratio by a mass spectrometer.

Before the processing of the samples can begin the entire system which includes the mass spectrometer and gas line, is degassed. This is done by vacuum pumping the system with multiple pumps until the entire amount of ^4He present within the system is

less than 1% of that expected to be released from the apatite crystals being analyzed. The samples are placed on a 25-holder disk where each one is heated and then measured separately. Between the He measurements from each sample a measurement of the amount of He in the blank is taken in order to ensure that He levels in the system are low enough to prevent contamination from the previous sample. This measured blank is subtracted from the subsequent sample that is measured. The average blank measurement in this study was 0.43 fmol.

A Neodymium/YAG laser is used to heat each platinum crucible that contains a single apatite crystal to 1050+/-15 °C. Each sample is heated in two stages: the initial primary degassing stage for 5 minutes, and a 5 minute re-heat to ensure the sample has been completely degassed. During the re-heat stage if any He is detected this probably indicates that inclusions in the sample had not been completely degassed during the first stage of heating or that the crystal is not apatite but a different mineral with a higher degassing temperature. Common mineral inclusions such as Zircon and Monazite would retain He through the first stage of heating due to their higher He retention temperatures.

The gases that are released from the samples during the heating are moved through a series of hydraulic valves and chambers through several filtering processes to the mass spectrometer. The goal of this process is for all released He to arrive as ultrapure He at the mass spectrometer in a single pulse.

Just before the ultrapure He gas reaches the mass spectrometer, each gas sample is spiked with 286 fmol of ^{3}He. The mass spectrometer measures the ratio of $^{3}He/^{4}He$ and is able to precisely measure the variance from the spike ratio caused by the additional ^{4}He

released by the sample. ^{2}He (as well as Hd (doubly ionized hydrogen), and deuterium (^{2}H) are also measured in order to avoid high levels that may cause interference.

In this study, two batches of samples were run automatically by a computer system from the heating to mass spectrometry measurements with two Durango standard samples each. Durango apatite standards have a known He age of 31.5 ± 1.6 Ma (2s) (Evans et al. 2005). The Durango apatite from the first batch of sixteen samples had a He weighted average age of 30.0 ± 1.3 Ma which falls within the accepted known age for the standard. The Durango from the second batch of eighteen samples had a He weighted average age of 35.0 ± 1.2 Ma which falls just outside the accepted range for Durango apatite standards.

3.7 Uranium Thorium Samarium Analysis

After the He gas measurements, the abundances of the parent isotopes; ^{238}U, ^{232}Th, and ^{147}Sm, were measured using an inductively coupled plasma mass spectrometer (ICP-MS) at the University of Kansas. A measurement of ^{235}U is not obtained because it is assumed to exist in natural isotopic abundance as a proportion of ^{238}U (^{235}U= ^{238}U/137.88; Evans et al. 2005). A solution of HNO_3 containing the spike of U Sm and Th is used to dissolve the apatite crystals while they are still in their platinum crucibles. This solution is diluted with a known amount of water and heated in an oven to ensure the entire crystal is dissolved. Using the ICP-MS the U, Th and Sm isotope ratios are measured to precisions <1-2% for most samples. Slight variations in spike volume and concentration are used for duplicate measurements of each sample. The expected amount of U-Th-Sm ranges from 10's to 1000's of ppm.

The dissolution of platinum crucibles may cause the formation of ions $^{194}Pt^{40}Ar^{+}$, $^{195}Pt^{40}Ar^{+}$, and $^{198}Pt^{40}Ar^{+}$ which cause interferences with isotopes of U with masses of 234, 235 and 238 respectively (Evans et al. 2005). Therefore, the ICP-MS signal is monitored at mass 234 as any increase in the natural abundance of mass 234 (0.0057%) is an indication of Pt interference. If necessary, interferences with masses 235 and 238, which are measured in this process, can be corrected using platinum isotope abundance ratios.

3.8 F_T Correction

As radioactive decay of the uranium and thorium decay series takes place in apatite crystals the alpha particles are emitted with kinetic energies of 4-8 MeV (Farley et al. 1996). As the alpha particles are emitted with high energy it takes between 11 μm to 34 μm (average 20 μm) for them to come to rest within solid crystals. This distance from the parent nucleus before the particles come to rest is called the stopping distance and the retention of He within the crystal depends on the proximity of the parent nucleus to the edge of the crystal. If the parent nucleus' distance from any edge exceeds the stopping distance then the alpha-particle will not escape the crystal regardless of it's trajectory. The probability that an alpha-particle will be ejected from the crystal increases as the parent nucleus lies with closer proximity to the crystal edge to a maximum of about 50% for a parent nucleus that lies on the grain edge. The relation between probability of retention and proximity to the grain edge and probability for retention is shown in Figure 3.6.

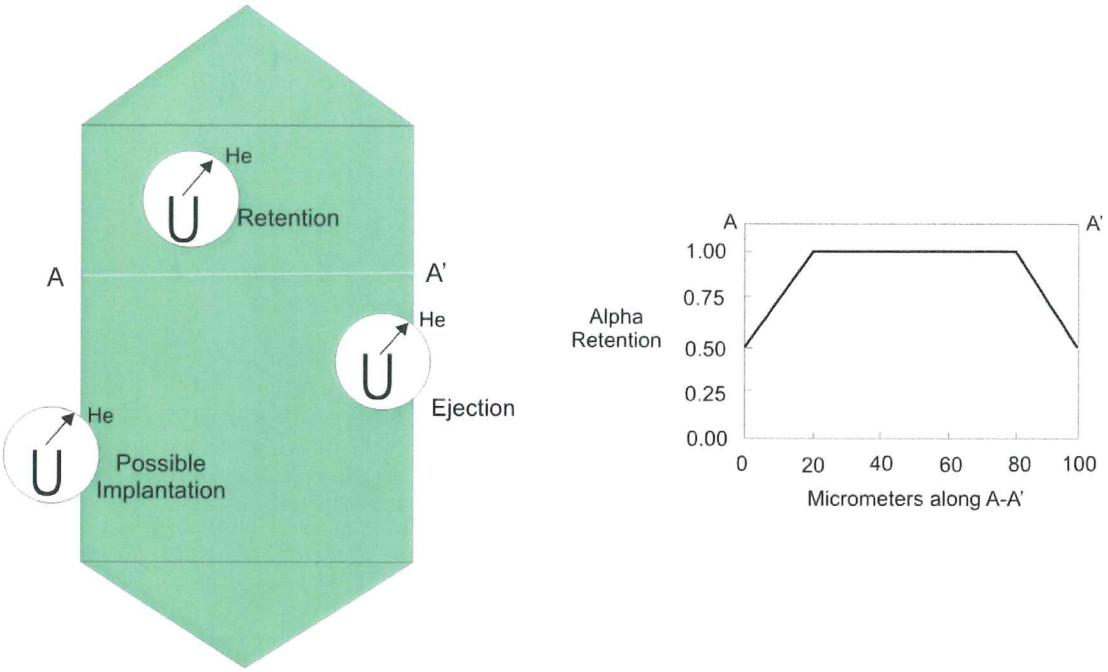

Figure 3.6: *The possibilities of alpha particle retention, ejection and possible implantation. Schematic 2D diagram on left shows parent nuclide locations denoted by U and the white circles show the possible extent an alpha particle will travel before coming to rest. "He" indicates locations where alpha particles may come to rest inside or outside a crystal. On the right is a plot showing how alpha retention will vary along the line A-A' or from rim to core to rim. Styled after Farley, 2000.*

A method was developed by Farley et al. (1996) to correct for He particle ejection. This model assumes a perfect hexagonal prismatic crystal shape, homogeneous distribution of U, Th and Sm parent nuclides, and that the implantation of alpha particles is negligible. The method developed by Farley et al. (1996) shows that measured ages must be divided by an F_T correction factor. This factor is calculated based on surface area to volume ratio (ß) and the stopping distance that is unique to each mineral and parent atoms (U,Th, and Sm). ß and F_T can be calculated for hexagonal prisms of apatite with the following equations.

$$ß = (2.31L+2R)/(RL) \quad (3.2);$$

Where L is the length of the hexagonal prism and R is half the distance between opposite apices of the hexagonal crystal face.

$$^{238}\text{U series: } {}^{U}F_T = 1 - 5.13ß^2 + 6.78ß \quad (3.3);$$

$$^{232}\text{Th series: } {}^{Th}F_T = 1 - 5.90ß^2 + 8.99ß \quad (3.4);$$

A mean correction must be calculated based on the relative amounts of U, Th, and Sm using the above F_T correction factors and the following equation.

$$\text{Mean } F_T = {}^{238}a\ {}^{U}F_T + (1 - {}^{238}a)\ {}^{Th}F_T \quad (3.5);$$

where ^{238}a is the fraction of He that is derived from ^{238}U.

The parameters that are used in the F_T correction have a bearing on the suitability of crystal geometry for He dating. Crystals must have a prismatic, elongate crystal habit with symmetry as close as possible to hexagonal in order to meet the parameters of the Farley et al. model and in order for ß to be a true surface area to volume ratio. Crystals must also be void of inclusions and zoning (as previously discussed in § 3.3) in order to have homogeneous distribution of U, Th and Sm.

3.9 He Age Determination

Measurements from laboratories were provided as individual ratios for each crystal of $^{235}U/^{238}U$, $^{230}Th/^{232}Th$, and $^{149}Sm/^{147}Sm$ which were converted to nuclei of radioactive elements using calculations laid out by Evans et al. 2005 (Appendix A). Measured He ages can be calculated using Eqn. 3.1 after calculating actual amounts of ^{238}U, ^{235}U, ^{232}Th, ^{147}Sm and ^{4}He. These calculations were carried out in MatLab using an algorithm created by Jose Antinao-Rojas, outputting calculated and corrected He ages for the entire set of samples. The results of the He ages are provided in § 4 and interpretations of the He ages are discussed in § 5.

3.10 Sources of Error

Each step of the (U-Th-Sm)/He method incorporates some error into the age calculation performed using equation 3.1. Each step of the measurement of He, U, Th and Sm incorporates some uncertainty (1-3%) which will affect the accuracy of measured He ages. Estimate of error from each analysis, U, Th and Sm, are provided by the University of Kansas and an estimate of 1.5-2% error in He measurements was selected upon consultation with K. Taylor of the Noble Gas Lab. The F_T correction also incorporates some uncertainty into the F_T corrected age as grain measurement incorporates error as do imperfect grains that are not perfect hexagonal inclusion free crystals with homogeneous distribution of parent isotopes (Ehlers and Farley, 2003). The uncertainty associated with the F_T correction greatly increases as grain size decreases and the magnitude of F_T corrections increases. The key sources of error have been incorporated into the error calculation (Eqn. 3.6) which calculates the total analytical error shown in Table 3.1 by adding all error sources in quadrature.

$$s = (U^2 + Th^2 + Sm^2 + He^2 + F_T^2)^{1/2} \qquad 3.6$$

Uncertainties in Measurements (%)						
Sample – Crystal Number	FT	U	Th	Sm	He	Total analytical error at 1σ
FT05-034b-4	9.2	1.9	0.6	0.6	2.0	9.7
FT05-034b-5	7.7	1.3	0.3	0.4	2.0	8.1
FT05-034b-10	4.5	1.2	0.5	0.2	2.0	5.1
FT05-034b-17	8.7	9.2	1.2	2.2	1.5	13.0
FT05-028-14	14.1	3.9	1.0	1.5	2.0	14.9
FT08-03-3	5.2	0.8	0.6	0.6	2.0	5.7
FT08-03-16	3.4	1.4	0.4	0.4	1.5	4.0
FT08-03-17	4.0	1.6	0.7	1.0	1.5	4.8
FT03-065-1	9.8	4.5	1.9	0.4	2.0	11.1
FT05-029-14	20.9	2.7	0.7	0.8	1.5	21.2
FT05-029-15	15.2	1.7	1.2	0.6	1.5	15.4
FT03-055-9	14.6	0.5	1.2	1.0	1.5	14.8
FT03-063-1	25.0	2.1	0.7	1.2	1.5	25.1

Table 3.1: *Quantitative uncertainty associated with measurements and F_T correction. The total analytical error is in the far right column.*

Additional error is associated with the measured ages due to properties that were not accounted for quantitatively. The additional error may come from imperfect crystal properties discussed in § 3.5 and these include the degree of rounding of a crystal and any small inclusions. The error may also come from uncertainty associated with (U-Th-Sm)/He dating and uncertainty in the half lives of radionuclides and the assumption that ^{235}U is equal to $^{238}U/137.88$.

Chapter 4: Results

4.1 Apatite crystal selection

Apatite crystal selection is an important part of the (U-Th-Sm)/He method and has a large influence on the quality of ages produced from samples. Of ca. 80 samples collected in the field for this study more than 50% did not yield sufficient apatite crystals of suitable size (>100 μm) and quality (devoid of inclusions) after the separation process. Of the samples that did contain apatite crystals the quantity and quality of these crystals varied.

4.2 Samples Used in this Study

Sample #	Description
FT03-038	Sample of coarse grained basaltic sill, Geodetic Hills area, blocks the valley to Fossil Forest. Intrudes finely laminated brown ss and siltstones.
FT03-046	Sample of coarse diorite sill, intrudes black shale of Triassic Blaa Mtn. Gp.
FT03-063	Sample of basaltic sill, dip 30SE, in the Eureka Pass area, medium grained.
FT03-055	Sample of sandstone, gray, cross-bedded, dip 30NE, Blaa Mtn. Gp, Triassic; very close to one of the rare basaltic dykes .
FT03-065	Sample of olivine-rich coarse basalt sill, 30-40 m thick, summit of Wolf Intrusion.
FT05-029	Sample of basaltic sill (Wolf Intrusion), close to SF03-66.
FT05-028	Sample of basaltic sill, SW of Colour Lake (Wolf Intrusion family).
FT05-034	Sample of basaltic sill, medium grained, within Little Matterhorn diapir complex .
FT05-036	Sample of 50cm bed of quartz sandstone within laminated siltstones (Triassic) west of Colour lake.
FT05-033b	Sample of quartz sandstone at foot off Little Matterhorn; (Christopher Fm, Cretaceous).
FT05-031	Sample of sandstone, Tertiary age, youngest exposed in syncline; Strand Bay Fm.
FT08-03	Sample of coarse white sandstone, NE side of island near AX5 reflector. Christopher Fm, Lower Mbr, Cretaceous.

4.3 (U-Th-Sm)/He ages

The crystal ages that were determined using apatite He dating in the crystals had a large range (Appendix B.) The youngest age determined in this study was 0 Ma and the oldest age was 16.0 Ga, these ages were rejected. Ages that were anomalously young or old were rejected; the basis of each rejection is outlined in Appendix B. The accepted ages in this study range between 12.5 Ma and 56.8 Ma (Table 4.1, Figure 4.2) and samples came from two distinct geographic locations, the Expedition Fiord Area and Geodetic Hills Area (Figure 4.1). Ages older than the age of crystallization of the formation sampled and ages that were older than any regional (U-Th-Sm)/He from Grist and Zentilli (2005) were rejected as the crystals tested may not have been apatite and the method of testing is only valid for apatite crystals. In some samples only one or two possible crystals which were less than ideal for the process were found to be analyzed. Photos of each crystal are shown in Appendix C, and it can be seen in the photos that some crystals did not have an ideal shape or were broken, these tended to produce inaccurate ages. The ages obtained from crystals that failed the He re-extract test (§ 3.5) were rejected due to the likelihood that these crystals contained zircon or monazite inclusions that would not be dissolved by HNO_3 before the ICP-MS and would therefore provide "parentless" He resulting in an anomalously old age (e.g. Farley, 2002; Grist and Zentilli, 2005.) Ages that were very young and had ^4He measurements less than the blank were rejected due to the uncertainty associated with the precision of a measurement that is less than the blank. Processes such as the He re-extract and blank measurement are put in place to ensure that the ages we compute are reliable and this information allows us to reject ages that fail these tests and are therefore judged unlikely to be correct and place confidence in ages that pass these test.

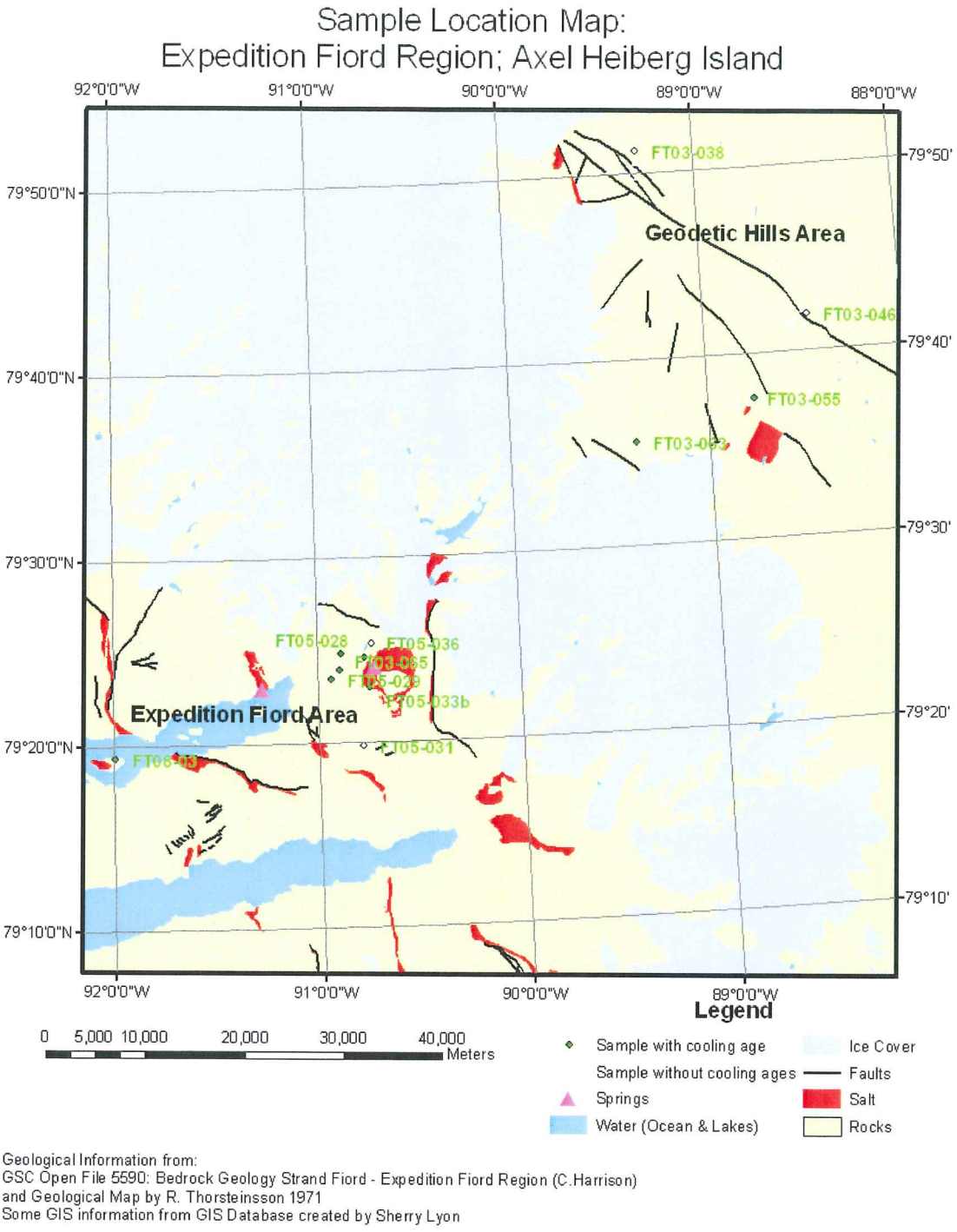

Figure 4.1: *Sample numbers plotted beside locations on Axel Heiberg Island in two geographic areas; Expedition Fiord and Geodetic Hills. Geology from Harrison and Jackson (2008).*

Sample	Mean L (μm)	Mean R (μm)	He (fmol)	U (ppm)	Th (ppm)	Sm (ppm)	Batch Number	Raw Age (Ma)	Mean FT	**Corrected Age ±2σ (Ma)**	**Weighted Average ±2σ (Ma)**
FT05-034b Sill (79.4105N, 90.76635W) 242 masl											
1*	292.5	39.4	3.70E+1	6.27E+00	2.62E+01	4.61E+02	0	25.2	0.67	**37.6 ± 3.0**	
2*	373.9	42.2	3.21E+1	8.77E+00	3.64E+01	6.38E+02	0	23.3	0.70	**33.3 ± 2.6**	
4	204	38.5	4.35E+0	7.60E+01	2.74E+02	6.00E+02	1	24.8	0.67	**37.0 ± 7.2**	**37.5 ± 4.5**
5	240	41.5	3.93E+0	1.24E+02	5.20E+02	1.24E+03	1	19.5	0.70	**28.1 ± 4.6**	
10	230	52.5	1.44E+1	2.77E+02	1.24E+03	2.84E+03	1	42.3	0.75	**56.8 ± 5.8**	
17	207	39.5	1.32E+0	6.85E+01	3.64E+00	2.31E+01	2	10.5	0.60	**17.5 ± 4.5**	
FT05-028 Sill (79.41402N, 90.8799W) 382 masl											
14	149	32	5.90E+0	7.30E+01	2.76E+02	7.66E+02	1	14.1	0.61	**23.3 ± 7.0**	
b1*	338.3	31.2	3.12E+0	5.95E+00	1.93E+01	4.61E+02	0	22.4	0.62	**36.1 ± 2.8**	**32.7 ± 3.5**
b2*	181.5	34.8	3.48E+0	4.46E+00	1.53E+01	3.56E+02	0	19.7	0.62	**31.8 ± 2.6**	
FT08-03 Sandstone (79.32317N, 91.992133W) 18 masl											
3	276	49.5	2.47E+0	3.81E+01	6.75E+02	1.33E+03	1	9.3	0.74	**12.5 ± 1.4**	
16	198	59.5	1.66E+0	114.9774	2.5917	15.97444	2	10.9	0.76	**14.3 ± 1.4**	**13.9 ± 1.4**
17	240	55	2.2E+09	91.0595	2.1406	14.24501	2	11.1	0.76	**14.7 ± 1.4**	
FT03-065 Sill (79.39867N, 90.89067W) 210 masl											
1	199	37.5	2.17E+0	7.35E+01	3.27E+02	8.49E+02	1	25.9	0.66	**39.0 ± 8.6**	**39.0 ± 8.6**
FT05-033b Sandstone (79.383N, 90.74W) 155 masl											
1*	273.3	58.7	2.53E+0	9.84E+00	1.99E+01	2.63E+02	0	31.3	0.76	**41.2 ± 3.2**	**40.5 ± 3.2**
2*	209.7	47.6	5.73E+0	2.45E+01	5.17E+01	5.03E+02	0	28.3	0.71	**39.9 ± 3.2**	
FT05-029 Sill (79.39082N, 90.93183W) 85 masl											
14	98	27	4.45E+0	1.04E+10	5.37E+10	1.37E+11	2	14.7	0.53	**27.9 ± 11.8**	**38.2 ± 13.6**
15	120	31	8.43E+0	1.17E+10	5.24E+10	1.42E+11	2	26.7	0.58	**45.6 ± 14.1**	
FT03-055 Sandstone (79.6259N, 88.7661W) 483 masl											
9	190	31.5	1.37E+1	3.61E+11	1.26E+11	8.49E+09	2	29.7	0.61	**48.6 ± 14.4**	**48.6 ± 14.4**
FT03-063 Sill (79.59303N, 89.36498W) 707 masl											
1	167	25	1.55E+0	1.9E+10	8.63E+10	2.6E+11	2	29.9	0.53	**56.0 ± 28.2**	**56.0 ± 28.2**

Table 4.1: *Complete results of accepted ages from the apatite (U-Th-Sm)/He method obtained from Expedition Fiord area. Rejected ages are discussed in Appendix B . The weighted averages in the far right column are displayed spatially in Figure 4.2 and are used for discussion in Chapter 5. *Analyst A. Grist.*

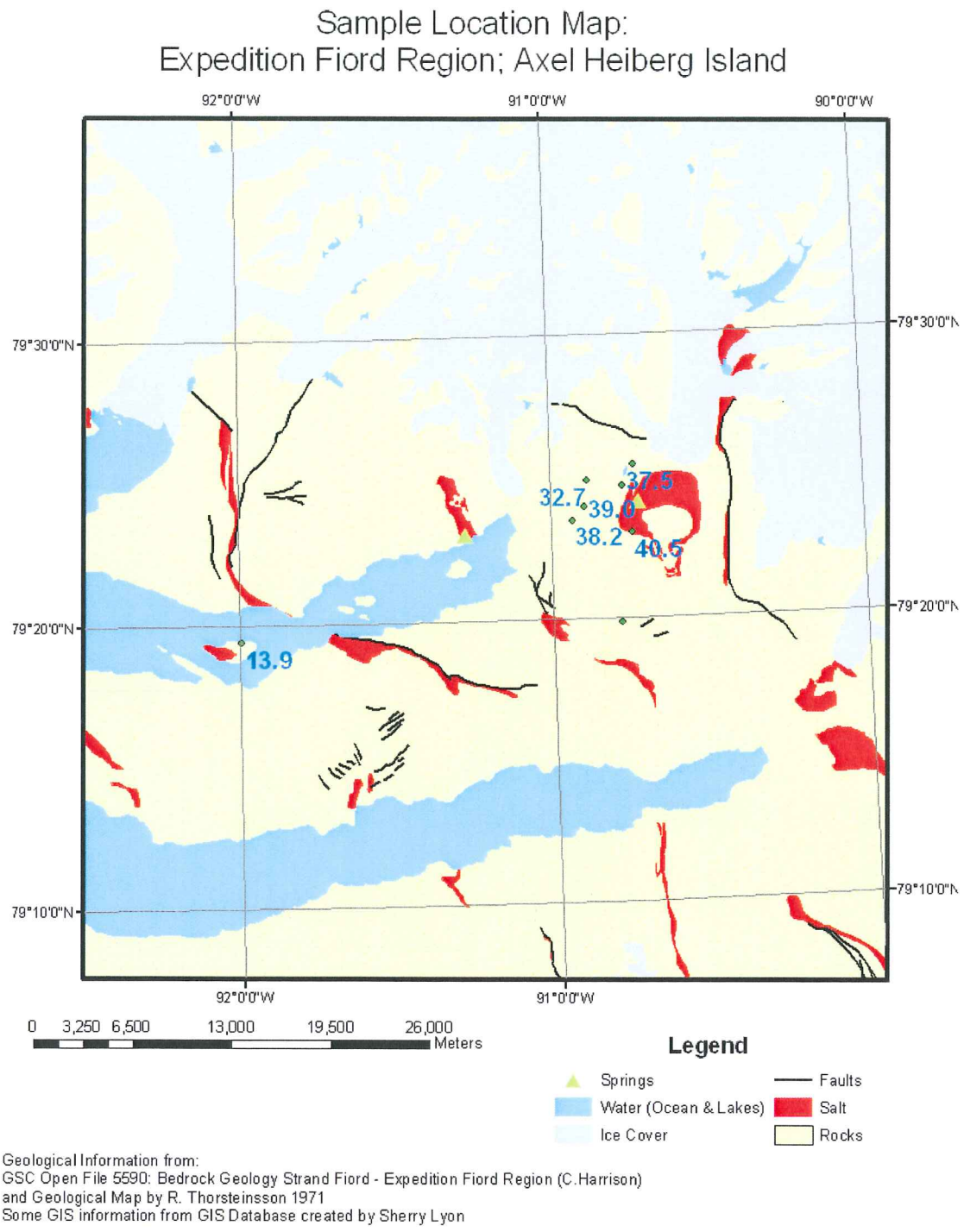

Figure 4.2: *He ages plotted beside sample locations on Axel Heiberg Island. Geology from Harrison and Jackson (2008).*

SAMPLE #	Latitude N	Longitude W	masl	AFT Age	ZFT Age	AHe Ages	Age of Stratigraphy
FT03-038	79.85372	89.2924	468	75 ± 6.6	120 ± 7		120
FT03-046	79.6989	88.47577	648	51.6 ± 5.5	117 ± 11		120
FT03-063	79.59303	89.36498	707	48.1 ± 4.7	118 ± 8	56.0 ± 28.2	120
FT03-055	79.6259	88.7661	483	60.3 ± 3	164 ± 6	48.6 ± 14.4	200-251
FT03-065	79.39867	90.89067	210	41.4 ± 3.8	79 ± 8	39.0 ± 8.6	~90?
FT05-029	79.39082	90.93183	85	41.4 ± 3.8	79 ± 8	38.2 ± 13.6	~90?
FT05-028	79.41402	90.8799	382			32.7 ± 3.5	~90?
FT05-034b	79.4105	90.76635	242			37.5± 4.5	~90?
FT05-036	79.42287	90.73075	189				200-251
FT05-033b	79.38305	90.74003	142			40.5 ± 3.2*	~100
FT05-031	79.33033	90.78167	728				~ 60?
FT08-03	79.32322	91.6588	18			13.9 ± 1.4	~100?

Table 4.2: *Samples from the study area and their apatite fission-track (AFT), zircon fission-track (ZFT) and apatite (U-Th-Sm)/He ages (AHe). AHe age with asterix (*) analyzed by A. Grist. AFT and ZFT ages are computed "central ages" from radial plots after Galbraith (1990). AFT dates analyzed in Dalhousie Fission Track Research Laboratory. ZFT dates were done by P. O'Sullivan of Apatite to Zircon, Inc. of Moscow Idaho, USA.*

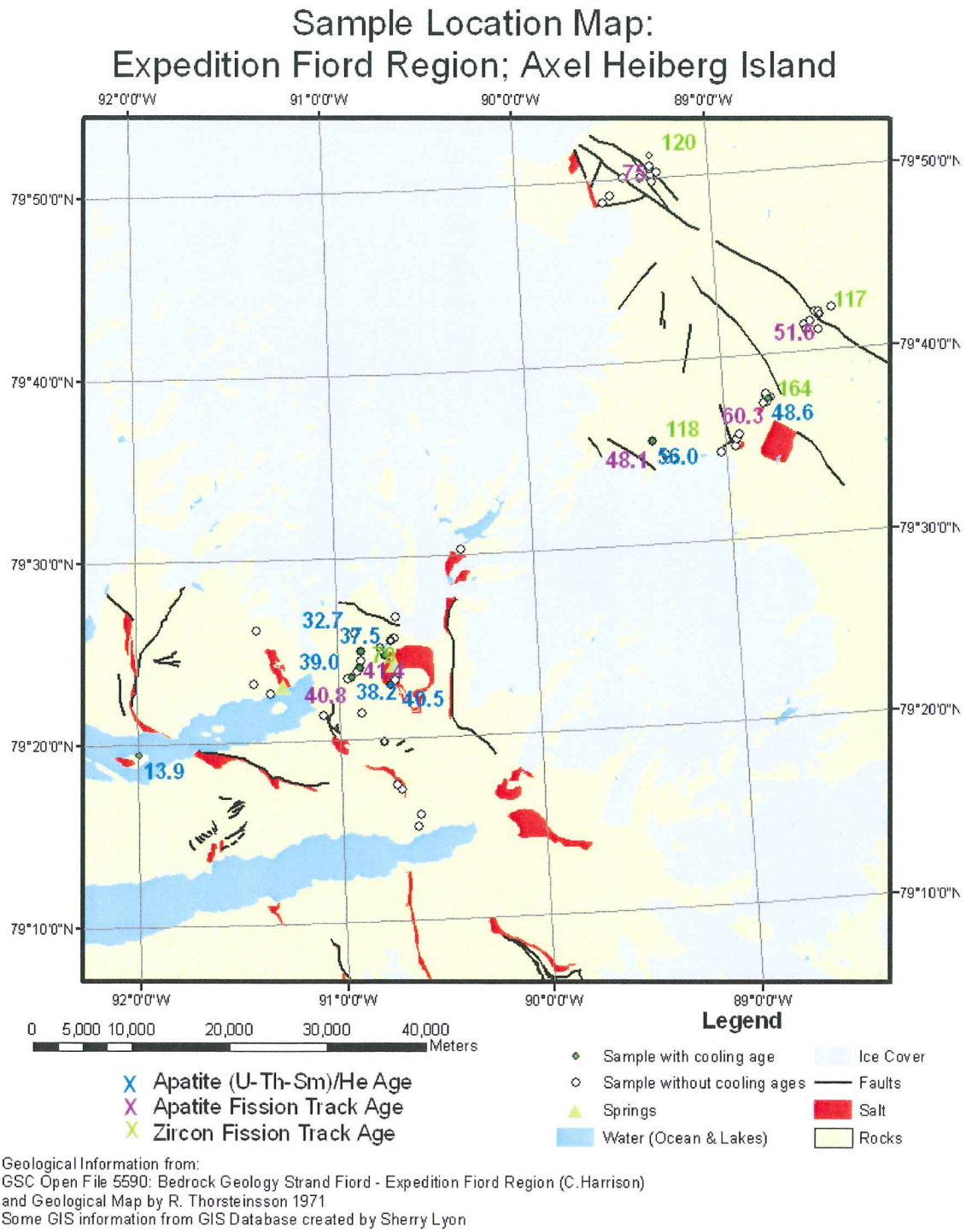

***Figure 4.3**: Sample location map with apatite fission-track (violet), zircon fission-track (green) and apatite (U-Th-Sm)/He ages (blue). Geology from Harrison and Jackson (2008). Ages are associated with green sample locations, perennial springs are symbolized with light green triangles and exposed salt is in red.*

4.4 Analysis of data

Thirteen apatite He cooling ages were obtained from seven samples by the writer in this study. An additional six apatite He cooling ages were obtained for three samples by Alexander Grist of the Dalhousie Geochronology Centre. The results from these analyses are combined in Table 4.1. As all samples were processed for He at the Dalhousie Geochronology Centre by K. Taylor and for U-Th-Sm at the University of Kansas by D. Stockli all methods are consistent. For this reason the ages should be reliable and are used for comparisons and interpretations in this study. The ages are consistent as can be seen in Table 4.1, sample FT05-034b analyses by A. Grist obtained ages of 33.3 ± 2.6 and 37.6 ± 3.0 on two grains while analyses by the writer obtained comparable ages of 37.0 ± 7.2, 28.1 ± 4.6 and 56.8 ± 5.8. The weighted average for this sample from A. Grist is 35.4 ± 2.8 Ma and the weighted average from He ages for this sample in this study is 39.5 ± 6.3 Ma, these weighted average ages are within the same range at a confidence of 2σ. The equations used to calculate weighted average and weighted standard deviation are shown in Appendix A, the weighted average calculation is used because it places less importance on ages that have more error with the goal of having a more accurate average age.

Chapter 5: Discussion & Interpretations

5.1 Organization of Discussion and Interpretations

The results of this study are first discussed as individual or groups of samples, and later regionally. For dates referred to in this chapter refer to Tables 4.1 and 4.2 and Figures 4.1, 4.2 and 4.3. It is evident that a larger number of samples and analyses is needed to reach more robust interpretations.

5.2 Discussion of individual samples

5.2.1 Samples FT03-038, FT03-046, FT03-063

These samples were dated with the apatite fission-track (AFT) method by A. Grist and represent tholeiitic basaltic sills in the Eureka Pass and Geodetic Hills areas of the Princess Margaret Range, where they intrude Triassic sediments of the Blaa Mountain Group. This group of sills yields a zircon fission-track (ZFT) age of ca. 120 Ma, therefore they belong to the oldest set of Cretaceous sills (the younger being ca. 90 Ma). Their AFT age is ca. 60 Ma. If this age represents cooling due to exhumation, and the geothermal gradient was approximately 37°C/km (Andersen et al. 2001), these rocks (now at the surface), were 3-4 km below the surface at 60 Ma. This cooling age is interpreted to represent uplift and exhumation of the hanging wall of the Stolz Thrust during the Eurekan Orogeny (e.g. Arne et al. 1998; Zentilli et al. 2008).

5.2.2 Sample FT03-055

This is a sample from the area of Eureka Pass. It is of sandstone from the Blaa Mountain Fm, which belongs to the Triassic, thus its absolute age is between 251 to 200 Ma (geological scale of ICS; Gradstein and Ogg, 2004). The sample was collected in the

vicinity of the older set of basaltic sills, and therefore was thermally affected at ca. 120 Ma (see above). The ZFT age is 164 ± 6 Ma, Jurassic, but the AFT age is 60 ± 3 Ma, reflecting the same age of Eurekan Orogeny exhumation cooling as the basalt sill samples discussed above; FT03-038, FT03-046, FT03-063.

5.2.3 Samples FT03-065, FT05-029, FT05-028, FT05-034

These samples are from basaltic sills of the younger age group, mainly represented by the thicker Wolf Intrusion. The ZFT age of samples FT03-065 and FT05-028 is 79 ±8 Ma. The AFT age of these samples is 41.4 ± 3.8 Ma, substantially younger than the AFT ages in the Eureka pass region to the northeast. The weighted He average ages obtained for samples FT05-028 and FT05-034 are 32.7 ± 3.5 Ma and 37.5 ± 4.5 Ma respectively but there is significant variation (Table 4.1).

5.2.4 Samples FT05-036, FT05-033b, FT05-031

These three samples were taken from sandstones. Sample FT05-033b is a quartz sandstone from the Cretaceous aged Christopher Fm, collected from Little Matterhorn, a major diapiric structure (Fig 1.1). The apatite He age obtained for this sample, analyzed by A. Grist, is 40.5 ± 3.2 Ma. The He age obtained for sample FT05-036 (7229± 622 Ma) as well as the ages from sample FT05-031 (16040 ± 5250 Ma, 12252 ± 3404 Ma) are much older than the He ages from the Sverdrup Basin and considered geologically meaningless. These data were rejected; the crystals dated were most probably not apatite or contained undetected uranium-rich inclusions (e.g. zircon) that were not dissolved during analysis for U, Th and Sm.

5.2.5 Sample FT08-03

This sample was taken near sea level at the western end of the thesis area, from an island in Expedition Fiord. The sampled strata belong to the Cretaceous aged Christopher Fm, and the island is dominated by a small evaporite diapir (see Figure 4.1) The apatite He weighted average age is 13.9 ± 1.4 Ma which is significantly younger than any other ages in the Expedition Fiord region. More samples from the western part of the thesis area are needed for comparison with this sample in order to make interpretations of this anomalously young age.

5.3 Implications of ages

All of the accepted He ages from this study (FT03-065, FT05-028, FT05-034b, FT05-033b, FT08-03, FT05-029) from the Expedition Fiord area of the eastern Sverdrup Basin are younger than the regional eastern Sverdrup Basin ages determined by Grist and Zentilli (2005) (Fig 5.1). These He ages from the Expedition Fiord area are also younger than the ages from the Geodetic Hills area (FT03-055, FT03-063) determined in this study. This local young age effect is also shown by apatite fission-track ages. As apatite He ages indicate a cooling through the 75°C isotherm (e.g. Farley, 2002) it can be concluded that the rocks present on the surface of the Expedition Fiord area cooled later than the rocks of the eastern Sverdrup Basin.

The anomalously younger apatite He cooling ages from sample FT08-03 may be the result of analytical error or evidence that the rocks of the western island cooled in the Neogene (Miocene-Pliocene). If this is the case they may have been exhumed later than the rest of the region to the east, or there was some unexplained thermal effect in the

western Expedition Fiord area. Without more analyses in the western area from moresamples the question cannot be resolved.

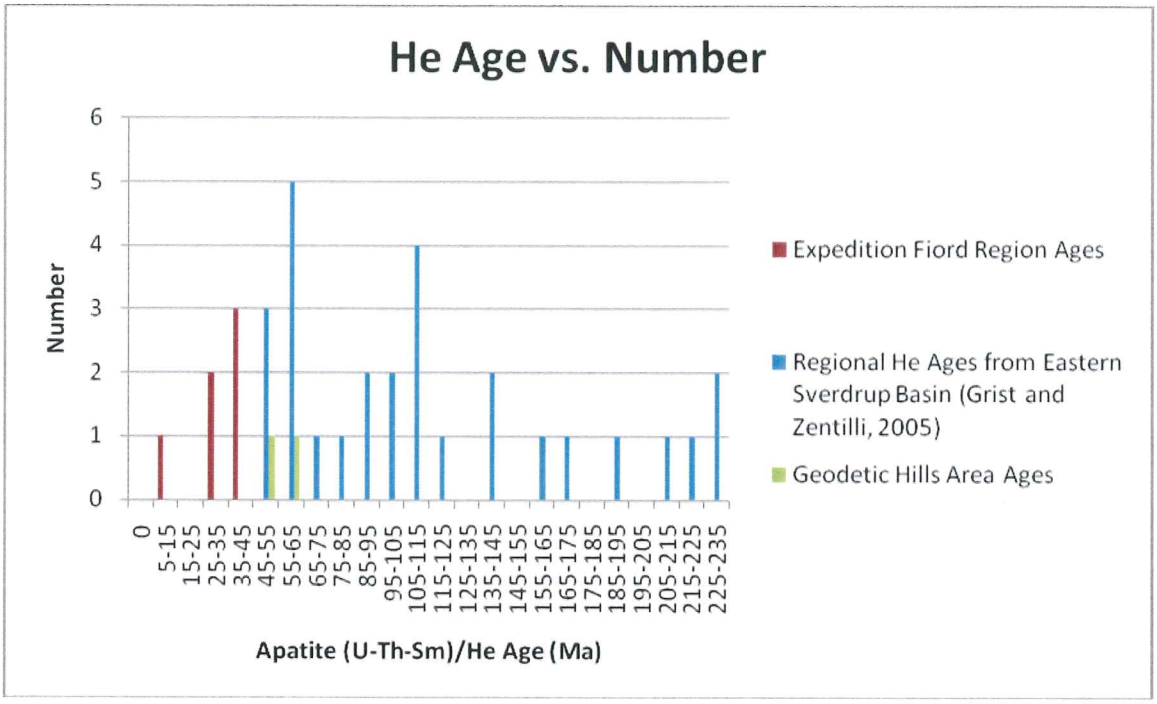

Figure 5.1: *Plot of He age vs. Number in order to compare regional ages from the eastern Sverdrup Basin from Grist and Zentilli (2005), to ages determined in this study for the Expedition Fiord Region. Note that all Expedition Fiord ages are younger than values from the Geodetic Hills Area as well as regional values.*

There may be several explanations for the observed age contrast between Expedition Fiord and the rest of the eastern Sverdrup Basin: 1) It is possible that the rocks on Axel Heiberg Island were exhumed at a later time than rocks in other parts of the basin, 2) It may be that the area where the ages are relatively younger is located in an area with a higher heat flow than the rest of the basin. Since there is no known volcanic activity in the area younger than ca. 90 Ma, (Villeneuve and Williamson, 2003) possible explanations for a thermal effect may be associated with the proximity to salt structures, the action of heat advection by warm fluids, or both.

5.4 Possibility of later exhumation of Expedition Fiord

The regional He ages determined by Grist and Zentilli (2005) date the time at which the rocks currently on the surface of the Sverdrup Basin passed through the 75°C isotherm during basin inversion associated with the Stolz Thrust of the Eurekan Orogeny. The Stolz Thrust is located to the west of Expedition Fiord in the Geodetic Hills area (Fig 1.1) and in order for exhumation of the rocks at Expedition Fiord to occur 5-10 Ma later than the Eurekan Orogeny, such as the rocks in the Stolz Thrust area; a tectonic event would be required to cause this exhumation. It is unlikely that a tectonic event in this area caused later exhumation of the rocks at Expedition Fiord although it is a possibility. The geological map (e.g. Harrison and Jackson, 2008) shows that Tertiary rocks of the Strand Bay and Iceberg Formations are deformed in the cores of synclines. These deformed formations are Late Paleocene to Middle Eocene (approximately 59 - 47 Ma; Figure 7 in Harrison et al. (1999), thus older than the Buchanan Bay Formation (Middle Eocene; ca. 46 - 41 Ma in Fig. 7 in Harrison 1999)). The Buchanan Bay Formation occurs NE of the Stolz Thrust and represents sediments shed during advance of the Stolz Thrust. The young Buchanan Bay Formation yields Eocene AFT ages characteristic of the Eurekan Orogeny (Zentilli et al. 2008) while the rocks found at Expedition Fiord, that are older than this formation, show younger AFT ages post-Eurekan orogeny . There is no tectonic activity recognized after the Middle Eocene in Axel Heiberg Island. Therefore the post Middle Eocene ages obtained in the thesis area, the head of Expedition Fiord are highly anomalous. Because this area is underlain by the salt canopy of Jackson and Harrison (2006) the possibility exists that the salt structure led to continued exhumation in the canopy domain. This hypothesis is a possibility and Zentilli and Williamson (2004) have

suggested that the evaporite diapirs in this region have risen since ice withdrawal from the area 10,000 years ago, and are probably rising to this day. M. Zentilli and P. Budkewitsch of the Canadian Centre for Remote Sensing have installed a total of 9 radar reflectors in 2007 and 2008 to test this hypothesis using radar satellite interferometry although there are no results yet.

5.5 Possible causes of thermal imprint

Possible mechanisms to explain the anomalous thermal signature discovered in the thesis area may include topographic variations or paleotopography, increased igneous activity in this area in relation to the rest of the eastern Sverdrup Basin, a thermal effect from an individual salt diapir, a thermal effect due to the underlying salt canopy, or an effect due to perennial springs. These possibilities are discussed sequentially below.

5.5.1 Topography variations or paleotopography

As discussed in chapter two, apatite He ages are strongly influenced by surface topography and due to exhumation, rocks found at the peak of a mountain should have cooled through the 75°C isotherm earlier than rocks at the base of the mountain (Fig 3.2; Ehlers and Farley, 2003.) For this reason there is often a linear relationship between older He age and higher elevation that can be used to estimate exhumation rates (Braun, 2002.) In this study only four ages were determined and there appears to be a negative trend between elevation and age with older ages occurring at the lowest elevations (Fig 5.2.) This pattern can be interpreted to indicate that the present day surface relief is smaller than it was when the rocks now at the surface crossed the closure temperature isotherm (e.g. Braun, 2002.) Braun's paper explains this trend as follows: *"For the rocks that will be collected at the top of ridges, relief reduction leads to a shortening of the distance*

travelled between the time the rocks crossed the closure temperature and the time they reached the surface. Conversely, the rocks found at valley bottoms will see that distance increase (in comparison with the case where relief remains constant). This leads to a reduction in apparent age at the ridge tops and an increase in apparent age at the valley bottoms and, thus, a counter-clockwise rotation of the age elevation relationship." (Braun, 2002) A relative planation of the topography after the Eurekan Orogeny (which created high mountains) seems to be supported by the existence of Pliocene-Pleitocene gravels on angular unconformities deposited over regional paleosurfaces (e.g. Harrison et al. 1999). Changes in relief explain the pattern observed within local ages but is not the cause of anomalously young ages in the Expedition Fiord region as the samples with younger ages in this region were taken at similar elevations as the rocks that cooled significantly earlier from the Geodetic Hills area.

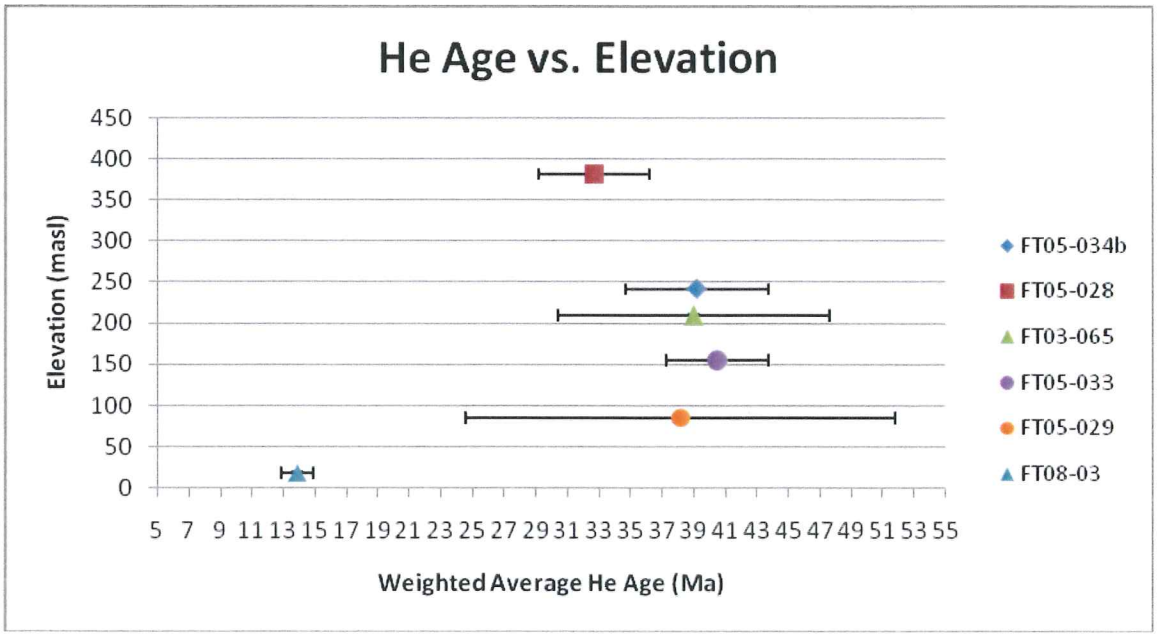

Figure 5.2: *Plot of age vs elevation of the samples from Expedition Fiord. Error is shown at 2s . The decreasing age with elevation indicates that the surface relief when the rocks reached the surface was less than what the relief was when the rocks crossed the 75°C isotherm. Note Sample FT08-03 does not show general trend as it is anomalously young age.*

5.5.2 Increased igneous activity

The largest volume of igneous rocks of Mesozoic age have been identified in the western Axel Heiberg Island region of the Sverdrup Basin, and as the thermal profiles for basins with significant magmatic components are affected by heat introduced by intrusive and extrusive igneous rocks this activity needs to be explored as a contributor to the thermal effect (Jones, 2006). The igneous rocks in the study area were deposited as hypabyssal lava flows, sills and dykes during two main pulses at ca. 130 and 90 Ma (Villeneuve and Williamson, 2003). Jones et al. (2007) explored the effects of magmatic events on the thermal history of the Sverdrup Basin using numerical modelling. Their models showed that the thermal effects from the emplacement of sills in the Cretaceous would not persist after the basin inversion caused by the Eurekan Orogeny (40 – 60 Ma). Therefore the increased igneous activity associated with the western Axel Heiberg Island area most likely did not have a persistent thermal effect that would cause a later cooling through the 75°C isotherm as compared to other areas within the eastern Sverdrup Basin. The thermal conductivity of basalt is 4-6 mW/°C (Table 2.1) which is higher than many of the rocks in the area and this could provide a minor contribution to the anomalously young ages observed at Expedition Fiord.

5.5.3 Salt diapirs

The exposed diapirs in the thesis area consist of anhydrite and gypsum, but elsewhere in the island (e.g. Stolz Diapir) halite is exposed; hence all diapirs are assumed to be underlain by salt; therefore the term salt is used as a general term (Jackson and Harrison, 2006). As salt is known to have a higher thermal conductivity than other sedimentary rocks (5.5 mW/°C; Table 2.1) and there are many exposed diapirs on the

surface of Axel Heiberg Island, one questions whether these diapirs may be linked to the observed thermal effect. The predicted effect on He ages by diapirs, a decrease in He age with proximity to a diapir, would be expected according to the thermal geometry indicated in Figure 3.3. However, only a weak relationship exists in the proximity of the diapirs on Axel Heiberg Island (Fig 5.3).

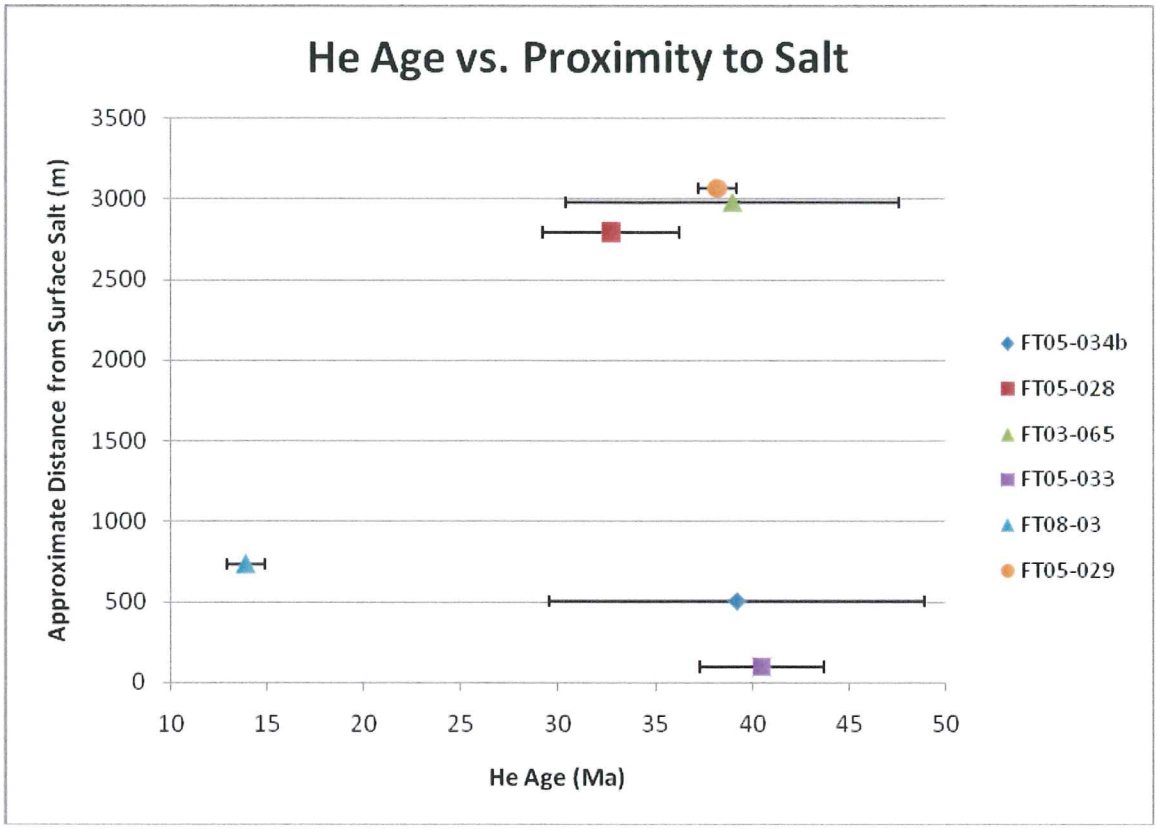

Figure 5.3: *Plot of He age vs. approximate distance from a surface salt diapir. Error is shown at 2*s *. Although there are only four data points there does not appear to be a clear trend associated with He age and distance from salt. The expected trend if individual salt structures thermally affect (U-Th-Sm)/He ages would be a decrease in He age with proximity to salt.*

As salt has the ability to funnel heat from surrounding rocks it can draw heat from rocks adjacent to the salt body and thermal anomalies should be focused in the region directly above a salt body (see section 2.3). The heat associated with diapirs needs to have a source, therefore, a deeply rooted diapir in hot rocks is required to have high thermal anomalies.

The samples taken on Axel Heiberg Island were taken from areas on the surface adjacent to diapirs as overlying sediments have been eroded from the tops of diapirs and they are exposed. The thermal focusing of heat through diapirs would indicate that individual diapirs most likely do not have a thermal effect on adjacent sediments rather this effect is pronounced in overlying sediments.

It is shown in Figure 2.5 that a diapir's thermal effect is most significant above and below the strucutre with very little effect adjacent to the structure. Samples for this study were taken adjacent to diapirs and for this reason it is unlikely that the observed thermal effect is due to individual diapirs.

5.5.4 Salt canopy

Jackson and Harrison (2006) interpreted the diapirs in the western Axel Heiberg Island area as second-generation diapirs rooted in a shallow allochthonous salt canopy (Fig. 2.6). A deeply rooted evaporite canopy could probably cause a thermal anomaly in overlying sediments through absorption of heat at depths that travels, preferentialy, through the canopy as a result of the salt's low thermal resistance. The samples from Expedition Fiord with anomalously young He ages all occur within the region of the salt canopy described by Jackson and Harrison (2006) (Fig. 5.4). The structural style of diapirs associated with the proposed salt canopy is only present in the western Axel Heiberg Area. The older eastern Sverdrup regional He ages are not taken from areas with diapir extrusion or known salt canopies. Therefore, it seems possible that the anomalously young He ages observed at Expedition Fiord could be caused by the underlying allochthonous evaporite canopy.

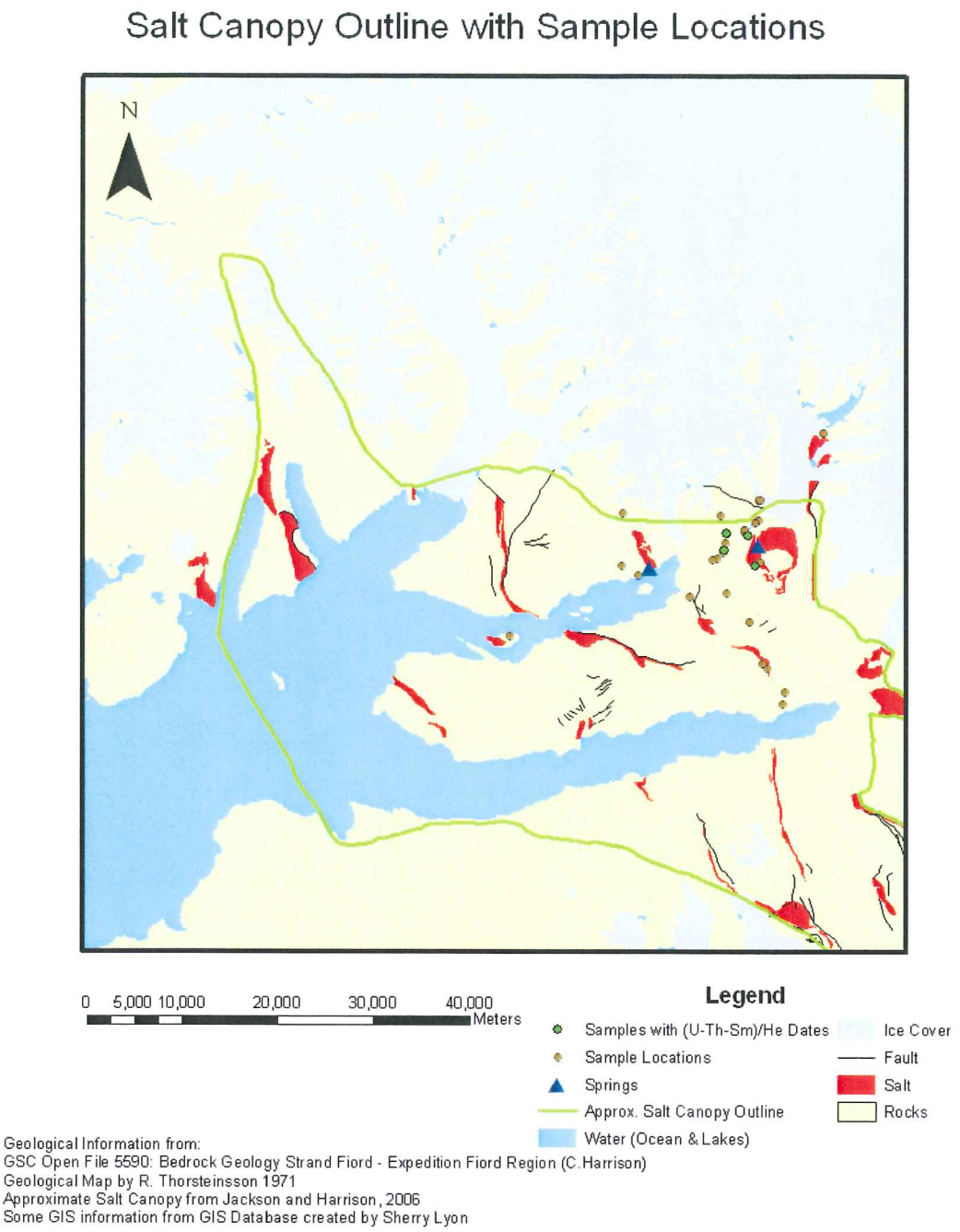

Figure 5.4: *Sample locations plotted within the area of the salt canopy. Sample locations where He ages were determined are shown with green circles and the approximate outline of a salt canopy is shown in green. The brown circles show sample locations where He dates could not be determined based on reasons discussed in chapters 3 and 4.*

The thermal effect of salt on sedimentary basins has been known for some time (e.g. Keen 1983, Keen and Lewis, 1982), and this phenomenon has been at the root of the

Dalhousie research project on Axel Heiberg Island since 2003 (Zentilli and Williamson, 2004). Numerical models confirming this effect on the isotherms in sediments are plentiful in the literature. For example, Yu et al. (1992) discuss the effect of salt on isotherms (Fig 2.5, Fig 5.5). One such model shows that above a salt sheet the tempereature profile is affected by the presence of salt but larger temperature perturbations are caused by the edge effect causing enhanced heat flux through sediments near the edge of a salt sheet. In other words, the temperature of sediments above a salt canopy will be increased as opposed to sediments not overlying a salt canopy and the temperature of sediments near the edge of a salt canopy will be further increased.

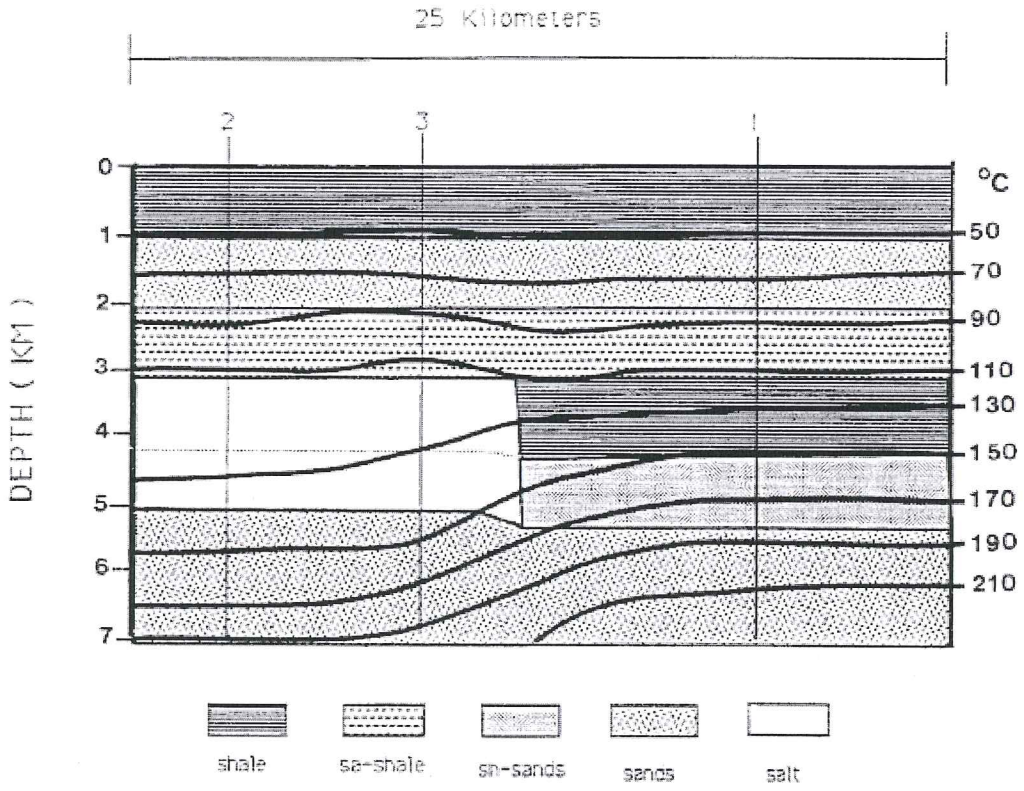

Figure 5.5: *The effect of a salt sheet on geothermal gradient. Heat flow is sensititve to lateral variations in conductivity which are prominent at the edge of a salt the sheet. The effect caused by a salt sheet or canopy is not as prominent vertically due to the scale of this figure and an enhanced heat flux is observed near the edge of the salt sheet. Figure from Yu et al. 1992.*

5.5.5 Perennial springs

Warm water perennial springs that are present in the Expedition Fiord area introduce warm fluids to the surface of Axel Heiberg Island (Fig 4.2, Pollard et al. 1999, Andersen et al. 2002) This fluid introduction is anomalous in that Axel Heiberg Island is a region of continuous permafrost (to ca. - 600 m) and springs that emit water at a constant flow rate and constant temperature year-round most likely have a deep geothermal source that is not affected by shallow events such as melting of glaciers and increased air temperatures in the summer or the freezing of lakes in the winter.

Andersen et al. (2002), proposed a model that describes the springs as a glacial phernomenon with the source of the springs being glacial lakes (see section 2.5; Fig. 2.7). Keen (1983) proposed the idea of hot fluids flowing through the zone of mechanical incompetence between a diapir and adjacent sediments as a migration pathway which had the effect of enhancing the thermal maturity of sediments overlying the Primrose Diapir, offshore Nova Scotia. Keen used numerical modelling in order to quantify the thermal maturity of the sediments observed at the Primrose Field and concluded that the high thermal conductivity of salt could not, by itself, cause the observed maturity as had previously been proposed. It appears that Keen's hot fluid model could explain the springs observed on Axel Heiberg Island.

For this reason the perennial springs are interpreted to support the interpretation that the anomalously young ages are due to the salt structures as the presence of these springs is interpreted to be, based on Keen's model, facilitated by the zone of mechanical incompetence adjacent to salt structures forming a pathway for these hot fluids.

It is possible that more than one factor is involved in producing the anomalously young (U-Th-Sm)/He dates in apatite encountered in the thesis area, and the writer prefers the hypothesis that the salt canopy and heat advection by fluids can better explain the data. However, as indicated above, the area underlain by the canopy may have been upwardly mobile and led to exhumation in post Eocene times.

Chapter 6: Conclusions and Recommendations

6.1 Conclusions

6.1.1 The rocks present at Axel Heiberg Island's Expedition Fiord Area of the eastern Sverdrup Basin have anomalously young apatite (U-Th-Sm)/He ages. These young ages mean that the rocks in this area passed through the 75°C isotherm later than other rocks of the eastern Sverdrup Basin.

6.1.2. These anomalously young ages are interpreted to be due to continued post-Eocene exhumation of the rocks in the canopy domain by the mobile salt at Expedition Fiord or a thermal effect.

6.1.3. Based on this study the writer concludes the most likely cause of anomalously young apatite He ages at Expedition Fiord is a thermal effect caused by fluid advection associated with an allochthonous salt canopy present in the Expedition Fiord Area.

6.2 Unanswered Questions and Recommendations for Future Work

This study was unable to determine an unequivocal reason for the younger He ages observed in the Expedition Fiord area of Axel Heiberg Island. For this reason brief descriptions of possible methods to test each hypothesis are explained.

The hypothesis that the anomalously young He ages are due to the salt structure causing continued exhumation in the canopy region is currently being tested. This is being done using radar satellite interferometry as discussed in section 5.4. The question whether the young ages are due to this movement remains unanswered but this hypothesis is already being tested and is therefore not discussed.

The thermal effect caused by the salt canopy could be tested by using the apatite He method to date rocks that are not underlain by a salt canopy and comparing the results to the He ages found in this study for rocks overlying the canopy. Using the apatite fission-track method to date the cooling of the rocks that are not underlain by the canopy through ~100°C could be used in addition to the He method in order to support the He data. If the thermal effect is an artifact of the allochthonous salt canopy then the observed He cooling ages from rocks above the canopy should be younger than the ages from rocks not underlain by the canopy, also an increased thermal effect producing slightly younger ages may be observed near the edges of the salt canopy due to the edge effect of salt.

This study did not determine if the thermal effect of salt diapirs can be detected using (U-Th-Sm)/He thermochronology. In order to test this effect samples from rocks overlying diapirs that have not been exposed on the surface could be obtained, as well as samples from rocks adjacent to these diapirs to observe differences in their cooling ages. Another way to test the thermal effect of salt diapirs would be to date samples from Cretaceous sills that are present within salt diapirs as the sills should have cooled through the 75°C isotherm much earlier than basin inversion and if the salt had a thermal effect the sills should show a younger cooling age than regional Sverdrup Basin rocks. Although in order for a thermal effect to be observed in the sills they must have been present near the top of the diapir as they passed through the 75°C isotherm as the thermal focusing of salt may draw heat from the sills themselves and transfer it to overlying sediments. It would also be expected that cooling ages of sills within the diapirs

themselves would be younger than cooling ages that may have been thermally influenced by a salt canopy.

Another important recommendation for future work is that more samples are taken from the western edge of the thesis area where a significantly younger cooling age was detected by sample FT08-03 in order to interpret the relevance and potential causes of this age.

REFERENCES

Andersen, D.T., Pollard, W.H., McKay, C.P., Heldman, J. 2002. Cold springs in permafrost on Earth and Mars. Journal of Geophysical Research. **107**: 41-47.

Arne, D.C., Zentilli, M., Grist, A.M. & Collins, M. 1998. Constraints on the timing of thrusting during the Eurekan Orogeny, Canadian Arctic Archipelago: an integrated approach to thermal history analysis. Can. Journal of Earth Sciences, **35**(1): 30-38.

Balkwill, H.R., Bustin, R.M., and Hopkins Jr., W.S. 1975. Eureka Sound Formation at Flat Sound, Axel Heiberg Island, and chronology of the Eurekan Orogeny. Geological Survey of Canada, Paper 75-1, Part B: 205-209.

Balkwill, H.R. Cook, D.G., Detterman, R.L., Embry, A.F., Hakansson, E., Miall, A.D., Poulton, T.P., and Young, F.G. 1983. Arctic North America and Greenland. M. Moullade and A.E.M. Narin (eds.). The Phanerozoic Geology of the World II; The Mesozoic, B, Elsevier Science Publishers, Amsterdam, p. 1-31.

Balkwill, H.R., and Fox, F.G. 1982. Incipient rift zone, western Sverdrup Basin, Arctic Canada, Memoir-Canadian Society of Petroleum Geologists, **8**: 171-187.

Braun, J. 2002. Quantifying the effect of recent relief changes on age-elevation relationships. Earth and Planetary Science Letters, **200**: 331-343.

Chen, Z., Osaztez, K.G., Embry, A.F., Gao, H., and Hannigan, P.K., 2000, Petroleum potential in western Sverdrup Basin, Canadian Arctic Archipelago, Bulletin of Canadian Petroleum Geology, **48**: 323-338.

Davies, G.R. and Nassichuk, W.W. 1991. Carboniferous and Permian history of the Sverdrup Basin, Arctic Islands, in H.P. Trettin, In Geology of the Innuitian Orogen and Arctic Platform of Canada and Greenland. *Edited by* H.P. Trettin. Geological Survey of Canada, Geology of Canada no.3, pp. 344-368.

Donelick, R.A. O'Sullivan, P.B. Ketcham, R.A. 2005. Apatite Fission-Track Analysis. In. Low Temperature Thermochronology: Techniques, Interpretations, and Applications. P.W. Reiners and T.A. Ehlers (eds). Reviews in Mineralogy and Geochemistry, **58**: 49-94.

Dunai, T.J. 2005. Forward Modeling and Interpretation of (U-Th)/He Ages. In. Low Temperature Thermochronology: Techniques, Interpretations, and Applications. P.W. Reiners and T.A. Ehlers (eds). Reviews in Mineralogy and Geochemistry, **58**: 259-274.

Ehlers, T.A. Farley, K.A., 2003. Apatite (U-Th)/He thermochronometry: methods and applications to problems in tectonic and surface processes. Earth and Planetary Science Letters **206**: 1-14.

Embry, A.F. 1991. Mesozoic History of the Arctic Islands. The Geology of the Innuitian Orogen and Arctic Platform of Canada and Greenland, H.P. Trettin (ed.). Geological Survey of Canada, Geology of Canada, no. 3. 369-436.

Evans, N.J., Byrne, J.P., Keegan, J.T., and Dotter, L.E. 2005. Determination of Uranium and Thorium in Zircon, Apatite, and Fluorite: Application to Laser (U-Th)/He Thermochronology. Journal of Analytical Chemistry, **12**:1159-1165.

Evans. R. 1977. Origin and significance of evaporites in basins around Atlantic margin. AAPG Bulletin. **61**(5): 783

Farley, K.A. 2002. (U-Th)/He Dating: Techniques, Calibrations, and Applications. In: Porcelli, D., Ballentine, C.J., and Wieler, R. (eds.) Noble gases in geochemistry and cosmochemistry. Reviews in Mineralogy and Geochemistry, **47**: 819-843.

Farley K.A., Stockli, D.F. 2002. (U-Th)/He Dating of Phosphates: Apatite, Monatite, and Xenotime. In: Phosphates: Geochemical, Geobiological, and Materials Importance. M.J. Kohn, J. Rakovan, and J.M. Hughes (eds.). Reviews in Mineralogy and Geochemistry, **48**: 559-578.

Farley, K.A., Wolf, RW., and Silver, LT. 1996. The effects of long alpha –stopping distances on (U-Th)/He ages. Geochimica et Cosmochimica Acta **60**: 4223-4229.

Fricker, P.E. 1963. Geology of the Expedition Area: Western Central Axel Heiberg Island Canadian Arctic Archipelageo. Jacobsen-McGill Arctic Research Expedition 1959-1962: 156pp.

Galbraith, R.F. 1990. The Radial Plot; Graphical assessment of spread in ages. Nuclear Tracks and Radiation Measurements. **17**: 207-214

Gradstein, F.M. and Ogg, J.G. 2004. Geologic time Scale 2004- why, how, and where next! Lethania. **37**: 175-181.

Grist, A.M. and Zentilli, M. 2004, Aspects of the thermal history of the eastern margin of Canada based on apatite fission-track and (U-Th)/He thermochronology. Dalhousie Ph.D Thesis. Copyright by Alexander M.Grist.

Grist, A.M. and Zentilli, M. 2005. The thermal history of the Nares Strait, Kane Basin, and Smith Sound region in Canada and Greenland: constraints from apatite fission-track and (U-Th-Sm)/He dating, Canadian Journal of Earth Science, **42**: 1547-1569

Harrison, J.C., and Jackson, M.P., 2008. Bedrock geology, Strand Fiord-Expedition Fiord area, western Axel Heiberg Island, northern Nunavut (parts of NTS 59E, 59F, 59G and 59H). Geological Survey of Canada, Open File 5590.

Harrison, J.C., Mayr, U., McNeil, D.H., McIntyre, D.J., Eberle, JJ., Harington, C.R., Chalmers, J.A., Dam, G. and Nohr-Hansen, H. 1999. Correlation of Cenozoic sequences of the Canadian Arctic region and Greenland; implications for the tectonic history of northern North America. Bull. Can Soc. Petroleum Geology, **47**, 223-254.

Hoen, E.W. 1961. A study of the gypsum diapirs of Axel Heiberg Island. Jacobsen-McGill Arctic Research Expedition to Axel Heiberg Island Queen Elizabeth Islands; Müller, B.S. (ed). McGill University, Preliminary Report pp. 161-170

Jackson, M. P. A., & Harrison, J. C. 2006. An Allochthonous Salt Canopy on Axel Heiberg Island, Sverdrup Basin, Arctic Canada. Geology (Boulder), **34**(12): 1045-1048.

Jones, S.F., 2006. Impact of magmatism on hydrocarbon systems of the Sverdrup Basin, Canadian Arctic Islands, Nunavut; a numerical modeling experiment. Bachelor of Science Thesis, Dalhousie University, Halifax, Nova Scotia. pp. 123

Jones, S., Wielens, H., & Williamson, M. 2007. Impact of Magmatism on the Petroleum System of the Sverdrup Basin, Canadian Arctic Islands, Nunavut; a Numerical Modeling Study; Journal of Petroleum Geology, **30**: 237-256.

Juez-Larre, J. 2003. Post Late Paleozoic Tectonothermal Evolution of the northeastern margin of Iberia, assessed by Fission-track and (U-Th)/He analysis. Vrije Universiteit Amsterdam.

Keen, C.E. 1983. Salt Diapirs and Thermal Maturity: Scotian Basin. Bulletin of Canadian Petroleum Geology. **31**: 101-108.

Keen, C.E. and Lewis, T. 1982. Radiogenic heat production in sediments from the continental margin of eastern North America: implications for petroleum generation. American Association of Petroleum geologists Bulletin. **66**: 1402-1407

Lyon, S.A., 2005. Geoscience applications of geographic information systems for the Strand Fiord area, west Axel Heiberg Island, Nunavut. Bachelor of Science Thesis, Dalhousie University, Halifax, Nova Scotia. pp. 92

Thorsteinsson, R. 1974.Carboniferous and Permian Stratigraphy of Axel Heiberg Island and Western Ellesmere Island, Canadian Arctic Archipelago. Bulletin - Geological Survey of Canada **224**: 115pp.

Thorsteinsson, R., and Tozer, E.T. 1970. Geology of the Arctic Archipelago. Geology and economic minerals of Canada. ed. Douglas, R.J.W. Geological Survey of Canada, Economic Geology Report 1. 547-590

Trettin, H.P. 1989. The Arctic Islands. Ch. 13. The Geology of the Innuitian Orogen and Arctic Platform of Canada and Greenland, H.P. Trettin (ed.). Geological Survey of Canada, Geology of Canada, no. 3.

Vermeesch, P., Seward, D., Latkoczy, C., Wipf, M., Gunther, and D., Baur, H. 2007. Alpha-Emitting mineral inclusions in apatite, their effect on (U-Th)/He ages, and how to reduce it. Geochimica et Cosmochimica Acta, **71**:1737-1746.

Villeneuve, M. and Williamson, M-C. 2003. 40Ar/39Ar Dating of mafic magmatism from the Sverdrup Basin magmatic province. Fourth international Conference on Arctic Margins, Programs/Abstracts: **45**.

Williamson, M.C., Jackson, H.R., Villeneuve, M., Larsen, L.M., Zentilli, M. 2004. GSC Atlantic collaborative projects and their significance for hydrocarbon exploration in the Canadian Arctic Islands and in the Davis Strait. Atlantic Geoscience Society Abstracts **40**: 165.

Yu, Z., Lerche, Y. I., & Lowrie, A. 1992. Thermal Impact of Salt; Simulation of Thermal Anomalies in the Gulf of Mexico. Pure and Applied Geophysics, **138**: 181-192.

Zentilli, M., Wielens, H., Grist, A.M., Kettanah, Y., Negulic, E., Brown, E.T., 2008. Thermal Effects of Salt on the Petroleum System: Evidence from Fission track Thermochronology, Fluid Inclusions and Basin Modelling. Central Atlantic Conjugate Margins Conference, Program & Abstracts **1**: 33-34.

Zentilli, M., Williamson, M.C. 2004. GSC Significance of salt diapirs, magmatism, and tectonics on the thermal history of Axel Heiberg Island, Nunavut. Atlantic Geoscience Society Abstracts **40**: 168.

APPENDIX A: Equations used in this study

1. Equation used to determine the He age from amount of U, Th, Sm, and He nuclei:

$$^{4}He = 8\ ^{238}U\ (e^{\wedge}(\lambda_{238}t) - 1) + 7\ (^{235}U/137.88)\ (e^{\wedge}(\lambda_{235}t) - 1) + 6\ ^{232}Th\ (e^{\wedge}(\lambda_{232}t) - 1) + {}^{147}Sm\ (e^{\wedge}(\lambda_{147}t) - 1)) \quad (3.1);$$

where λ is the decay constant for the parent atoms ($\lambda_{238} = 1.551 \times 10^{-10}\ y^{-1}$, $\lambda_{235} = 9.849 \times 10^{-10}\ y^{-1}$, $\lambda_{232} = 4.948 \times 10^{-11}\ y^{-1}$, $\lambda_{147} = 6.539 \times 10^{-12} y^{-1}$) and **t** is the time (years) (Farley, 2002).

2. Ft Correction equations:

$$ß = (2.31L+2R)/(RL) \quad (3.2);$$

Where ß is the surface area to volume ratio, L is the length of the hexagonal prism and R is half the distance between opposite apices of the hexagonal crystal face.

$$^{238}U \text{ series: } {}^{U}F_T = 1 - 5.13ß^2 + 6.78ß \quad (3.3);$$

$$^{232}Th \text{ series: } {}^{Th}F_T = 1 - 5.90ß^2 + 8.99ß \quad (3.4);$$

$$\text{Mean } F_T = {}^{238}a\ {}^{U}F_T + (1 - {}^{238}a)\ {}^{Th}F_T \quad (3.5);$$

3. Determination of U-TH-Sm nuclei from ratios for He age determination (Evans et al., 2005);

Determining # of ^{238}U Atoms from $^{235}U/^{238}U$ (Isotopic Ratio):

RU_{sa} = Isotopic ratio of the spiked sample (measured);

RU_{sp} = Isotopic ratio of calibrated spike (calibrated);

RU_{min} = Isotopic ratio of the mineral in nature (0.0072);

$RU_{standard}$ = Isotopic ratio of standard solution (calibrated);

RU_{sst} = Isotopic ratio of spiked standard solution (measured);

U_{ust} = Total # of ^{238}U atoms in the unspiked standard solution;

U_{sp} = Total # of ^{238}U atoms in spike;

Uc_{st} = Concentration of ^{238}U in the calibrated standard solution, ng/mL;

UV_{st} = Volume of ^{238}U of standard solution added, μL;

$^{238}U_{atoms}$ = # of ^{238}U in the sample;

$$^{238}U_{atoms} = {}^{238}U_{sp} * (RU_{sa} - RU_{sp})/(RU_{min} - RU_{sa})$$

$^{238}U_{sp}$ = # of ^{238}U in the spike;

$$^{238}U_{sp} = {}^{238}U_{ust} * (RU_{st} - RU_{sst})/(RU_{sst} - RU_{sp})$$

$^{238}U_{ust}$ = # of moles in the unspiked standard

$$^{238}U_{ust} = (Uc_{st}/238 * UV_{st}(10^3))*((1/RU_{st})/((1/RU_{st}) + 1))$$

Determining # of Th and Sm atoms from isotopic ratio:

RX_{sa} = Isotopic ratio of the spiked sample (measured);

RX_{sp} = Isotopic ratio of calibrated spike (calibrated);

RX_{sst} = Isotopic ratio of spiked standard solution (measured);

X_{ust} = Total # of X atoms in the unspiked standard solution;

X_{sp} = Total # of X atoms in spike;

Xc_{st} = Concentration of x in the calibrated standard solution, ng/mL;

XV_{st} = Volume of X of standard solution added, μL;

x = molecular weight of X (Th = 232, Sm = 149)

X_{atoms} = # of X in the sample;

$X_{atoms} = Abs(X * (RX_{sp} - RX_{sa})/(RU_{sa})$

X_{sp} = # of X in the spike;

$X_{sp} = X_{ust} * (RX_{sst})/(RX_{sp} - RX_{sst})$

X_{ust} = # of moles in the unspiked standard

$X_{ust} = (Xc_{st}/x * XV_{st} (10^3))$

4. Error calculation: Adding up uncertainties in quatrature

$$\sigma = (U^2 + Th^2 + Sm^2 + He^2 + F_T^2)^{1/2} \qquad 3.6;$$

5. Weighted Average

X= weighted mean

H= corrected He age

U=uncertainty

$X=(H_1*1/U_1 + H_2*1/U_2 + H_3*1/U_3 \ldots\ldots..)/ (1/U_1 + 1/U_2 + 1/U_3 .....)$

6. Weighted Standard Deviation

σ = standard deviation

X= weighted mean

U=uncertainty

$\sigma = X * (U_1 + U_2 + U_3 \ldots\ldots..)/ (1/U_1 + 1/U_2 + 1/U_3 .....)$

APPENDIX B: Complete Data List from (U-Th-Sm)/He Dating

The complete list of analyses completed in this study are shown below. Rejected ages are shaded gray with a reason for rejection shown in the far right column.

Sample	Mean L (μm)	Mean R (μm)	He (fmol)	U (ppm)	Th (ppm)	Sm (ppm)	Re-extract (y/n)-Batch Number	Raw Age (Ma)	Error	**Corrected Age ±2σ (Ma)**	
FT05-034b Sill (79.4105N, 90.76635W) 242 masl											
1*	292.5	39.4	3.70E+12	6.27E+00	2.62E+01	4.61E+02	n-0	25.2	0.04	**37.6 ± 3.0**	
2*	373.9	42.2	3.21E+12	8.77E+00	3.64E+01	6.38E+02	n-0	23.3	0.04	**33.3 ± 2.6**	
4	204	38.5	4.35E+09	7.60E+01	2.74E+02	6.00E+02	n-1	24.8	0.10	**37.0 ± 7.2**	
5	240	41.5	3.93E+09	1.24E+02	5.20E+02	1.24E+03	n-1	19.5	0.08	**28.1 ± 4.6**	
10	230	52.5	1.44E+10	2.77E+02	1.24E+03	2.84E+03	n-1	42.3	0.05	**56.8 ± 5.8**	
15	170	30.5	3.89E+09	8.76E+02	6.87E+00	2.63E+02	n-2	397.9	0.16	**585 ± 94**	Too old; older than emplacement
17	207	39.5	1.32E+09	6.85E+01	3.64E+00	2.31E+01	n-2	10.5	0.13	**17.5 ± 4.5**	
FT05-028 Sill (79.41402N, 90.8799W) 382 masl											
1	246	31	8.85E+08	7.18E+01	4.00E+02	7.41E+02	n-1	11.5	0.16	**18.5 ± 5.8**	Too young?
5	177	29.5	1.04E+09	9.73E+01	3.72E+02	9.77E+02	y-1	18.3	0.17	**31.1±10.8**	Failed re-extract
9	113	36	2.03E+10	1.15E+02	5.21E+02	1.30E+03	n-1	290.6	0.11	**468 ± 106**	Too old; older than emplacement
10	78	25	1.20E+08	1.42E+02	6.67E+02	1.49E+03	n-1	4.2	0.25	**8.6 ± 4.4**	Too young?
14	149	32	5.90E+08	7.30E+01	2.76E+02	7.66E+02	n-1	14.1	0.15	**23.3 ± 7.0**	
b1*	338.3	31.2	3.12E+07	5.95E+00	1.93E+01	4.61E+02	n-0	22.4	0.04	**36.1 ± 2.8**	
b2*	181.5	34.8	3.48E+07	4.46E+00	1.53E+01	3.56E+02	n-0	19.7	0.04	**31.8 ± 2.6**	
FT08-03 Sandstone (79.32317N, 91.992133W) 18 masl											
3	276	49.5	2.47E+09	3.81E+01	6.75E+02	1.33E+03	n-1	9.3	0.06	**12.5 ± 1.4**	
7	300	61.5	1.20E+07	3.33E+01	5.41E+02	9.66E+02	n-1	0.0	0.04	**0.04 ± 0.004**	Too young; He measured less than blank
8	191	45.5	1.81E+07	1.27E+00	3.15E+01	0.00E+00	y-1	2.8	0.09	**3.9 ± 0.6**	Failed re-extract
16	198	59.5	1.66E+09	114.9774	2.5917	15.97444	n-2	10.9	0.04	**14.3 ± 1.4**	

17	240	55	2.2E+09	91.0595	2.1406	14.24501	n-2	11.1	0.05	**14.7 ± 1.4**	
FT03-065 Sill (79.39867N, 90.89067W) 210 masl											
1	199	37.5	2.17E+09	7.35E+01	3.27E+02	8.49E+02	n-1	25.9	0.11	**39.0 ± 8.6**	
2	248	34.5	1.46E+09	1.21E+02	5.70E+02	1.15E+03	n-1	9.8	0.13	**15.1 ± 38**	Too young
FT05-033b Sandstone (79.383N, 90.74W) 155 masl											
1*	273.3	58.7	2.53E+00	9.84E+00	1.99E+01	2.63E+02	n-0	31.3	0.04	**41.2 ± 3.2**	
2*	209.7	47.6	5.73E+00	2.45E+01	5.17E+01	5.03E+02	n-0	28.3	0.04	**39.9 ± 3.2**	
FT05-036-1 Sandstone (79.42287N, 90.73075W) 189 masl											
1	168	41.5	2.06E+11	1.88E+01	1.13E+02	6.10E+00	n-1	4924.8	0.68	**7229 ± 1244**	Too old- zircon; older than emplacement
FT05-031 Sill (79.33033N, 90.7816W) 728 masl											
1	114	22.5	2.52E+11	2.18E+01	1.70E+02	3.06E+01	n-1	7656.0	0.48	**16040 ± 10500**	Too old- zircon? Older than emplacement
4	339	24	9.97E+11	6.15E+01	1.92E+02	5.43E+01	y-1	6627.4	0.54	**12252 ± 6808**	Too old- zircon? Older than emplacement
FT05-029 Sill (79.39082N, 90.93183W) 85 masl											
1	118	18.5	4.33E+08	8.48E+09	3.42E+10	7.7E+10	y-2	20.0	0.50		Failed re-extract
14	98	27	4.45E+08	1.04E+10	5.37E+10	1.37E+11	n-2	14.7	0.21	**27.9 ± 11.8**	
15	120	31	8.43E+08	1.17E+10	5.24E+10	1.42E+11	n-2	26.7	0.15	**45.6 ± 14.1**	
FT03-055 Sandstone (79.6259N, 88.7661W) 483 masl											
8	138	25.5	3.23E+09	1.95E+10	6.98E+09	0	n-2	0.0	0.25	**0.00 ± 0.00**	Unreasonable
9	190	31.5	1.37E+11	3.61E+11	1.26E+11	8.49E+09	n-2	29.7	0.15	**48.6 ± 14.4**	
11	135	41.5	3.79E+09	1.6E+10	6.98E+09	18060000	y-2	1.9	0.12	**2.79 ± 0.66**	Failed re-extract
13	144	28.5	2.24E+09	1.88E+10	6.98E+09	18060000	n-2	2.1	0.20	**3.72 ± 1.52**	Unreasonable
FT03-038 Sill (79.85372N, 89.2924W) 468 masl											
1	188	34	6020000	2.06E+09	1.88E+10	6.98E+09	n-2	0.7	0.13	**1.14 ± 0.29**	Unreasonable ages more analyses needed
5	154	34.5	6020000	1.87E+09	1.34E+10	6.98E+09	n-2	0.9	0.12	**1.49 ± 0.37**	
9	251	35	5.21E+09	2.07E+09	1.8E+10	5.23E+09	n-2	627.1	0.12	**958 ± 239**	
FT03-046 Sill (79.6989N, 88.47577W) 648 masl											
18	159	40	1.56E+09	1.97E+09	1.51E+10	6.98E+09	n-2	217.8	0.12	**325 ± 80.3**	Unreasonable ages more analyses needed
5	143	34	7.77E+08	1.42E+10	5.24E+10	2.17E+11	n-2	21.9	0.13	**35.3 ± 9.0**	
13	121	24.5	54180000	2.49E+09	1.73E+10	5.23E+09	n-2	6.5	0.27	**12.6 ± 6.85**	
FT03-063 Sill (79.59303N, 89.36498W) 707 masl											
1	167	25	1.55E+09	1.9E+10	8.63E+10	2.6E+11	n-2	29.9	0.25	**56.0 ± 28.2**	

APPENDIX C: Images of the Apatite Crystals analyzed for (U-Th-Sm)/He

Part 1: Crystals analyzed by the author R. Buckley.
Images of crystals analyzed for (U-Th-Sm)/He taken with a Zeiss Axioplan binocular microscope and PaxIt software. Sample number followed by crystal number is shown in the lower left corner of each photo while the radius of the crystal is shown in the lower right corner.

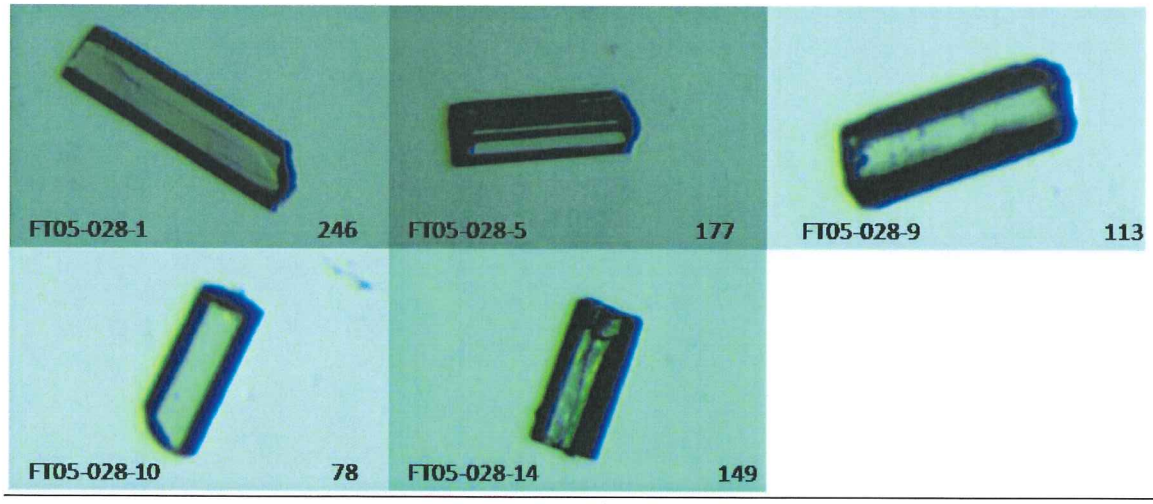

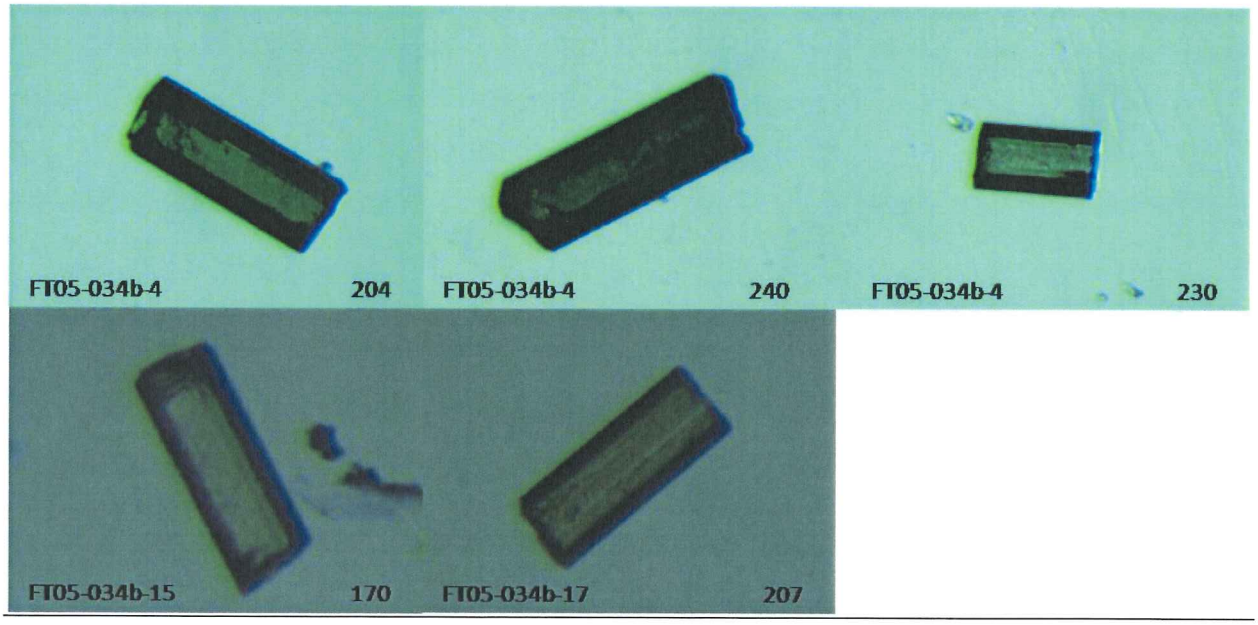

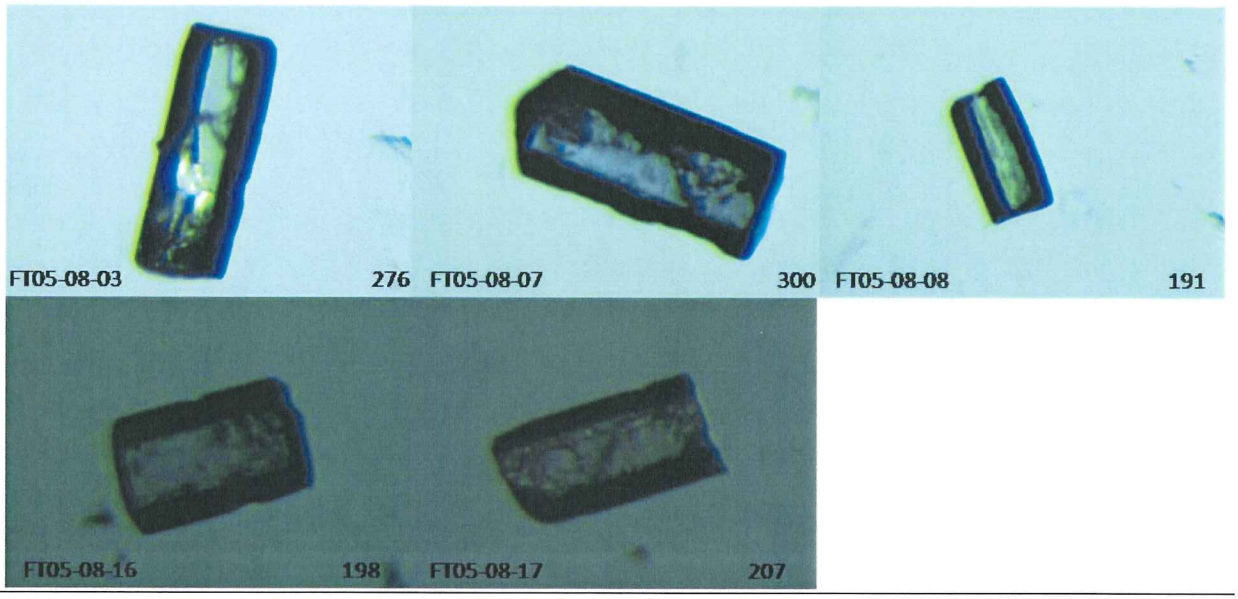
FT05-08-03 276
FT05-08-07 300
FT05-08-08 191
FT05-08-16 198
FT05-08-17 207

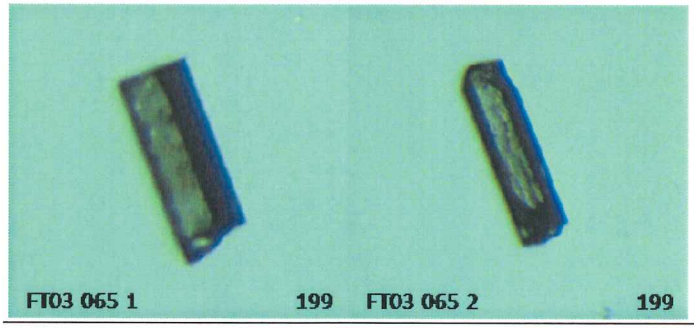
FT03 065 1 199
FT03 065 2 199

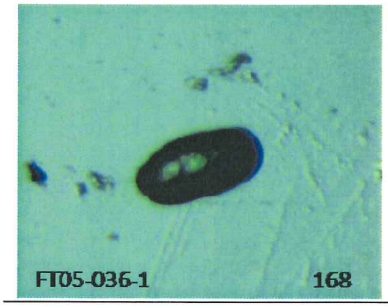
FT05-036-1 168


FT05-031-1 114
FT05-031-4 339

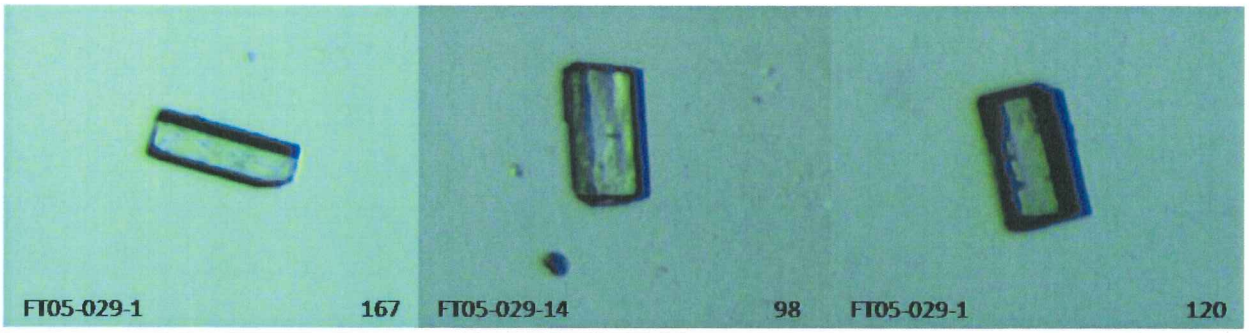
FT05-029-1 167
FT05-029-14 98
FT05-029-1 120

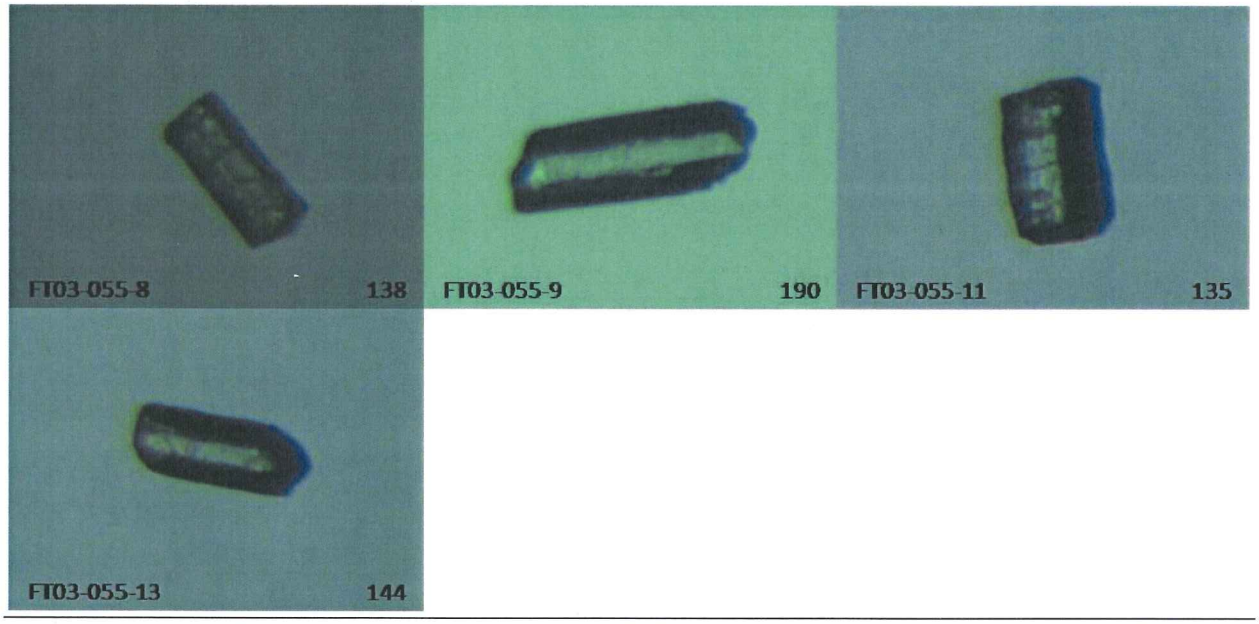
FT03-055-8 138
FT03-055-9 190
FT03-055-11 135
FT03-055-13 144

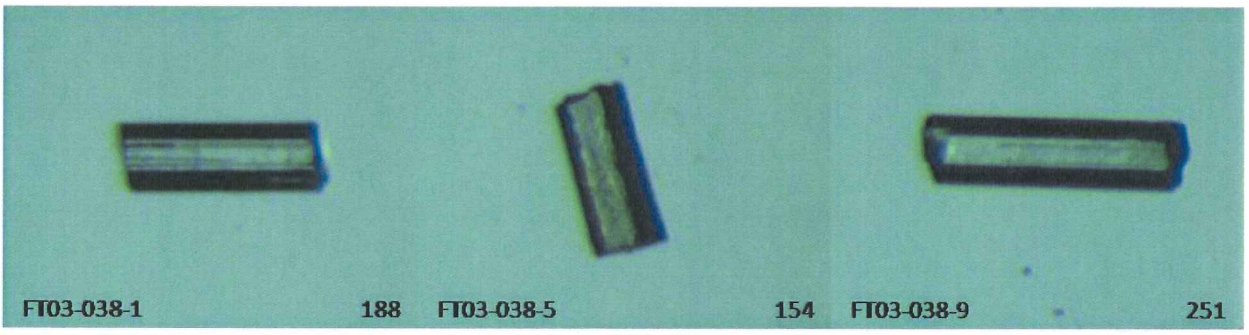
FT03-038-1 188
FT03-038-5 154
FT03-038-9 251

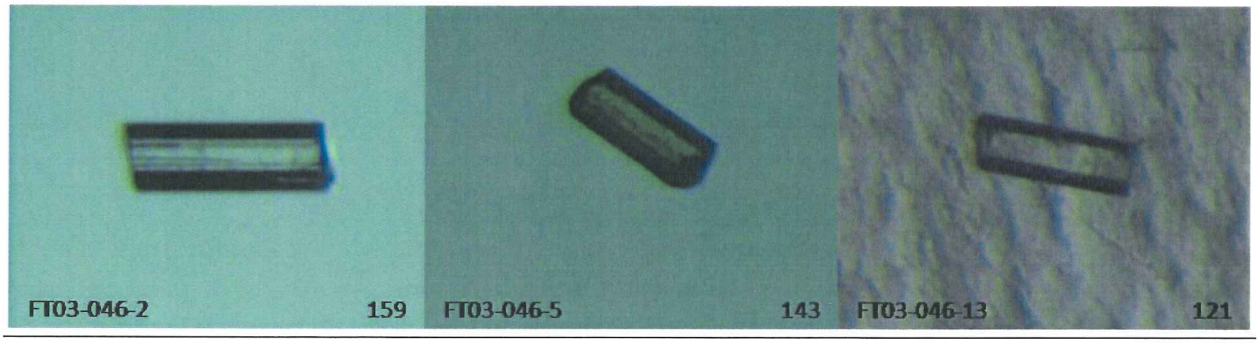
FT03-046-2 159
FT03-046-5 143
FT03-046-13 121

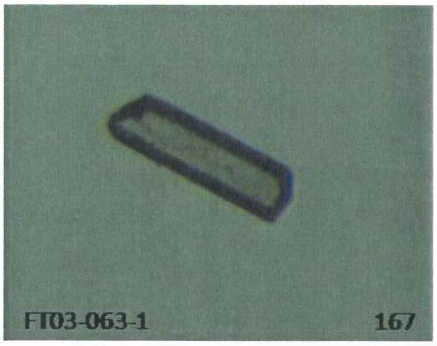

Part 2: Crystals analyzed by A. Grist in February, 2006. Sample number is at the top of photograph with a scale bar. More than one crystal was placed in each crucible for analysis and as such more than one crystal is included in the photo for each sample.

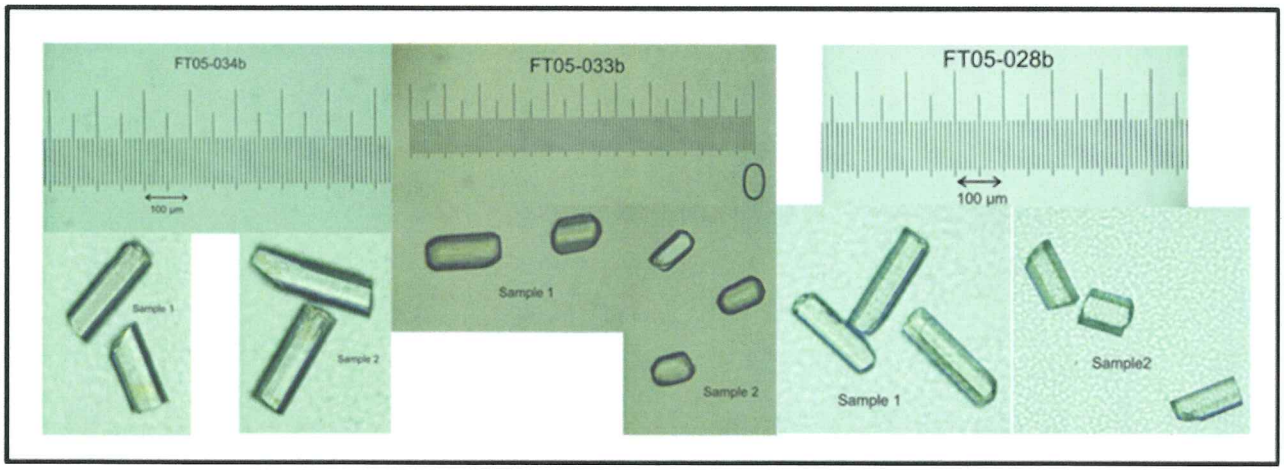

APPENDIX D: Geologic Time Scale

This is the time scale with which this thesis refers to and is from Gradstein and Ogg (2004).